

Reply to Reviewer #1

We would like to thank the reviewer for the supportive and helpful comments to improve our manuscript. Below we address the reviewer's comments in detail.

Comments from the Reviewer

- The reviewer suggested us to include some descriptions about the link between the developments presented in the manuscript and the tuning of the whole climate model

We added a new subsection that briefly describes tuning issues as follows.

3.11 Comments on tuning

At the end of this section, we give a brief description of the model tuning related to clouds. At a stage of developing schemes, a number of amip type simulations (with typical one-year length) were performed using atmospheric and aerosol coupled model, to check the basic behavior of schemes and the basic impacts on radiative fluxes. At a tuning stage, five-year runs of amip type simulations were mainly examined. The main targets for tuning parameters related to clouds in MRI-ESM2 were global-mean biases and root-mean square errors of shortwave and longwave radiative fluxes at the top of the atmosphere. The tuning parameters related to clouds are parameters which affect differently by cloud types and control cloud properties such as cloud cover, cloud water content, and cloud number concentration. In the stratocumulus parameterization (Section 3.1), the threshold value of ECTEI was tuned to increase Southern Ocean clouds as described in Section 4.1.3. The relatively large mode radius of sulfate of 0.10 μm (possible range: 0.05 – 0.10 μm) was chosen to obtain smaller cloud droplet number concentration to prevent an excessive aerosol-cloud interaction. Treatment of the WBF effect (Section 3.2), cloud overlap scheme (Section 3.5), schemes for ice sedimentation and ice conversion to snow (Section 3.9), and others (Sections 3.3, 3.4, 3.6, and 3.7) were not tuned. Descriptions of the model tuning (other than cloud-related parameters) are given in Yukimoto et al. (2019).

In addition, the possible range of ECTEI ($-3.0 - +3.0$ K) was specified in the first paragraph in Section 4.1.3.

- Minor comment: please specify the unit of the variables in section 4.2.1

It is true that the unit in the section is important information for readers, as the reviewer pointed out. Thank you. The unit was specified.

Reply to Reviewer #2

We would like to thank the reviewer for the supportive comments and helpful suggestions to improve our manuscript. In our new version of the manuscript we try to follow virtually all of the reviewer's suggestions. Below we address the reviewer's comments in detail.

Comments from the Reviewer

- there is absolutely no guarantee that these empirical relationships can be applied to climate change. In my opinion, this point clearly deserves some discussion.

We added a new section and discuss this issue briefly as follows:

4.1.4 Brief discussion on climate change simulations

It is well-known that changes in LCC in warmer climates cannot be explained by changes in LTS (e.g., Williams et al., 2006; Medeiros et al., 2008; Lauer et al., 2010). The mechanism of this discrepancy is also well-understood: inevitable decrease of moist adiabatic lapse rate in the free atmosphere in warmer climates causes increase in LTS (e.g., Miller, 1997; Larson et al., 1999), even though the inversion strength that probably contributes to determine LCC does not change (e.g., Wood and Bretherton, 2006; Caldwell and Bretherton, 2009). It was expected that an index EIS could avoid this problem and could be used for discussion of LCC changes under warmer climates because EIS is a more physics-based index that represents inversion strength at the cloud top more directly. However, more recently, it turned out that LCC tends to decrease, although EIS increases in warmer climates in most climate models (e.g., Webb et al., 2013). Subsequently, it was shown by Qu et al. (2014) that changes (including variations in the present climate and future changes) in LCC can be determined by a linear combination of changes in EIS (positive correlation) and SST (negative correlation). Kawai et al. (2017) derived the linear combination from the index ECTEI and showed that a decrease in LCC under increased EIS in warmer climates can be explained based on the ECTEI change (see Kawai et al. (2017) for more detail). It is true that a usage of empirical relationships obtained in the present climate for climate change simulations has a possibility of causing spurious climate feedback. On the other

hand, we would like to note that ECTEI is even more physics-based index than EIS, the relationship is not used directly for cloud formation but used as a threshold for cloud top mixing, and ECTEI can explain positive low cloud feedback, although the risk of spurious climate feedback still cannot be eliminated.

- 1. The partitioning of detrained cloud water into liquid and ice in MRI-ESM2 follows Hu et al. (2010). The same data by Hu et al. (2010) was also used to evaluate MRI-ESM2. It is found that the mass and the frequency ratio in Fig. 4 are both fairly close to the Hu et al. data. Thus overall, the WBF process appears to have a rather small influence (which might be partially explained by still using a mixing ratio threshold). Could you please briefly comment on this? Is the WBF process allowed to act on detrained cloud water in the same time step?

We understand that this could be a little confusing part. First, source terms (to which Hu et al. (2010) function is adopted) are not only detrainment from convection, but also formation of stratiform clouds due to upward motion and temperature decrease. Actually, in MRI-ESM2 (with the new parameterization), production of ice from these source terms are dominant, and contributions from depositional growth (and others including immersion freezing, condensation freezing, and contact freezing) are much smaller. Therefore, the ratio in Fig. 4 is close to the Hu et al. function that is used to divide source terms into ice and liquid. This means that WBF process that explicitly occurs in MRI-ESM2 is very weak. (However, a usage of Hu et al. (2010) function to determine the ratio of newly produced LWC promotes ice production in the case of IWC greater than a threshold in our treatment, and it means WBF process is parameterized in MRI-ESM2.) The following short sentence was simply inserted in the third paragraph in Section 3.2: “In MRI-ESM2, IWC production from the source terms of LWC based on partitioning using a function of Hu et al. (2010) is dominant, and the contributions from a depositional growth and other freezing processes are considerably small.”

- 2. Hu et al. (2010) present an empirical relationship that arises as a the consequence of a large number of physical processes. While the underlying physics remain the same, there is absolutely no guarantee that such a relationship will hold in a future climate. Updrafts and/or aerosol may influence such a relationship and they may change in a

systematic way.

The point is true. We added the following sentence in the last paragraph in Section 3.2: “It should also be noted that empirical relationships including the ratio curve of Hu et al. (2010) may not hold completely in a future climate because a large number of meteorological factors contribute to form such relationships and they may change in a systematic way.”

- 3. Many climate models show a decrease of cloud cover at the same time as LTS increases in a future climate. In a regional model, Lauer et. al 2010 (<https://www.doi.org/10.1175/2010JCLI3666.1>) also find that changes associated with global warming do not follow empirical relationships between LTS and cloud cover. Therefore, such empirical relationships should not be used in climate models.

The response to this comment is included in the response to the reviewer’s major comment.

- 4. I know that this would mean breaking a tradition, but I would be very interested in seeing a plot that shows the effect of the bug fixes mentioned in 3.7.

It is not easy to take back all the bugs and to convince our colleagues to spend computer resources to investigate influences of the bugs. Instead, the impact of the bug related to number concentrations of the cloud particles that is mentioned in Section 3.7 is shown in Fig. R1 (attached to this reply) for the reviewer (and the readers of this open discussion). The figure shows that the bug caused excessive reflection of solar radiation, particularly for stratocumulus and stratus over the subtropics and northern Pacific region for July.

- 5. Do the the changes due to the individual model modifications add up linearly to yield the final result? In Fig. 11, a plot could be added that compares the sum of the individual contributions to the difference between MRI-ESM2 and CGCM3.

We agree that it is an interesting issue. Actually, the sum of impacts from the individual model modifications described in this manuscript (in Fig. 11b) does not match the difference between MRI-ESM2 and CGCM3 (in Fig. 11c) so well. There are several

reasons for that. First, several bug fixes related to clouds significantly (as describes in the response above) contribute to the radiation flux bias. Second, modifications in some other physical processes, for example, convection parameterization contribute the radiation flux as well. Modifications in other component models, for example, the aerosol model (through changes in optical thickness of clear sky and optical thickness of clouds via changes in aerosol concentrations) contribute the radiation bias. In addition, there should be non-linearly on each impact from each modification. Therefore, we decided not to discuss this summation to avoid confusion and complexity.

- 6. Fig. 10 shows a strongly decreased time step dependency of the ice water content in MRI-ESM2 compared to MRI-CGCM3 which the authors attribute to the I2S conversion term. This seems very plausible to me. However, if I understand it right, in MRI-ESM2, the partitioning of IWC into $IWC > 100$ and $IWC < 100$ is still performed at every time step (according to Eq. S10), right? As far as I can see, in the absence of a threshold below which conversion from cloud ice to snow starts to be active, this could in principle still cause a problem similar to the one described in lines line 423f. Nevertheless, at least the time step dependence seems to be addressed. Without first looking at Fig. 10, I would have expected that in the case of a long-lived non-precipitating cloud the ice water path would still become depleted during a successive time steps because of this partitioning. And, on the other hand, does partitioning every time step mean that a part of the IWP will always be be particles smaller than 100 micrometer ($IWC < 100$)? Again, all of this seems less of a problem than what has already been addressed here.

The situation is a little complicated.

First, it is important to confirm that the ratio of Eq. (S10) is not used to actually (directly) determine the ratio of large ice and small ice in total IWC. Therefore, large ice production during one time step ($= C_{I2S} \Delta t$) (not $(1 - \alpha_i) q_i$) is basically proportional to Δt . (Note also that a ratio r_{iw} is in Eq. (2) but a ratio α_i is not in Eq. (6). If, for example, the ratio α_i is used as a substitute for r_{iw} in Eq. (2), similar timestep dependency is found.)

It is true that the ratio α_i is calculated from Eq. (S10) every time step. But it is used only to determine the conversion rate of small ice to large ice C_{I2S} (Eq. (5)). To determine the conversion rate, the ratio α_i calculated from Eq. (S10) based on observation (at the observation depth from the top of the cloud) should be used and the ratio calculated in the model that depends on model time step should not be used. For clarification, the following sentence was inserted after Eq. (6): “Note that although the ratio α_i obtained from Eq. (S10) is used to calculate the conversion rate C_{I2S} , it is not used to directly

determine the ratio between small ice crystals and snow differently from in Eq. (2).”

It is true that in the case of a long-lived non-precipitating cloud the ice water path would still become depleted if we don't introduce the conversion threshold. But it would occur regardless of the model time step.

- p. 2, l. 46: ratio of supercooled water -> ratio of supercooled water to cloud (liquid and ice) water

Corrected.

- p. 9, l. 281f: I completely agree on this (<https://doi.org/10.5194/gmd-2018-307-RC1>).

Thank you for your agreement. We are pleased to know that the reviewer recognizes the value of non-use of a lower limit of cloud droplet number concentration.

- **The advection term in Eqs. 2 and 6 is in flux form and not in advection form. In order to convert an advection equation to flux form, it is necessary to use the continuity equation. This implies that the flux form equation is valid in cases in which the tracer (here: ice) is advected with the flow. The flux form equation is not valid for sedimentation.**

The reviewer's comment is correct. The equations in the previous manuscript were not correct. (We wanted to make the equations easy to understand, though they were forms not actually used. But it is true that it is confusing.) The equations that we actually use are as follows:

$$\frac{\partial q_i}{\partial t} = C_g + \frac{R_i}{\rho_a \Delta z} - \frac{v_{ice}}{\Delta z} r_{iw} q_i - \frac{(1-r_{iw})q_i}{\Delta t} \quad (2)$$

$$\frac{\partial q_i}{\partial t} = C_g + \frac{R_i}{\rho_a \Delta z} - \frac{v_i}{\Delta z} q_i - D_{12S} q_i \quad (6)$$

where R_i ($\text{kg m}^{-2} \text{s}^{-1}$) is the ice sedimentation flux into the layer from above, and Δz (m) is the layer thickness. (This form is generally used for ice sedimentation calculation (e.g., Smith, 1990; Rotstayn, 1997).)

Therefore, we corrected these equations as noted above. Thank you for your insightful comment.

- p. 13, l. 396f: Morrison and Gettelman, 2007 (<https://www.doi.org/10.1175/2008JCLI2105.1>) use substepping.

Thank you for the information. The following sentence was inserted:

“Although adopting shorter time steps for selected processes that is called substepping (e.g., Morrison and Gettelman, 2008) would be an ideal solution, it can increase computational cost to some degree.”

- p. 15, l. 445f: this is not unavoidable. see my comment regarding l. 396f.

The sentence was modified as follows:

“Therefore, the sedimentation cannot be calculated appropriately with the time step used in our climate models, and the treatment of instant fall of snow (large ice) through to the surface is unavoidable, unless substepping is introduced.”

- Fig. 4, caption: should the Hu et al. data be compared to the mass or the frequency weighted ratio?

The part in the caption was clarified as follows:

“An observational curve from Hu et al. (2010) that corresponds to a frequency ratio”

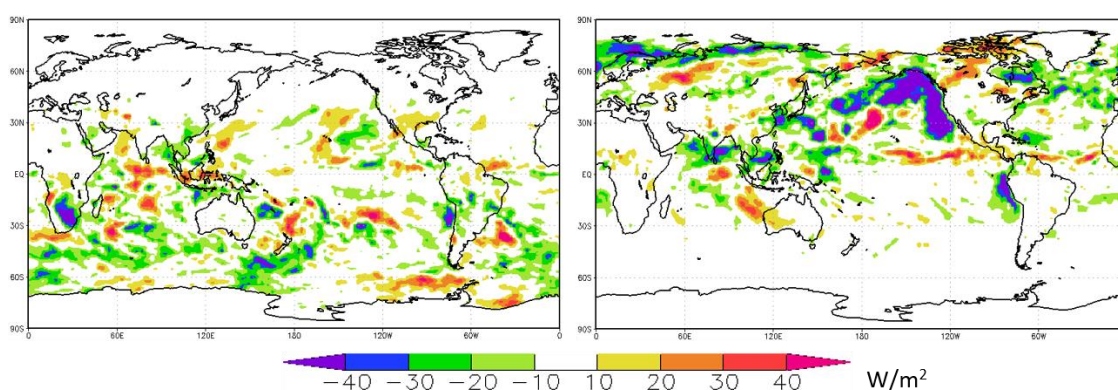


Figure R1. Impacts of a bug fix (bug fixed – with the bug) on TOA upward shortwave radiative flux (W m^{-2}) in amip type simulations for January (left panel) and July (right panel) in 2001.

1 **Significant Improvement of Cloud Representation in Global Climate** 2 **Model MRI-ESM2**

3 Hideaki Kawai¹, Seiji Yukimoto¹, Tsuyoshi Kosshiro¹, Naga Oshima¹, Taichu Tanaka¹, Hiromasa
4 Yoshimura¹, Ryoji Nagasawa¹

5 ¹Meteorological Research Institute, Japan Meteorological Agency, Tsukuba, 305-0052, Japan

6 *Correspondence to:* Hideaki Kawai (h-kawai@mri-jma.go.jp)

7 **Abstract.** The development of the climate model MRI-ESM2, which is planned for use in the sixth phase of the Coupled
8 Model Intercomparison Project (CMIP6) simulations, involved significant improvements to the representation of clouds from
9 the previous version MRI-CGCM3, which was used in the CMIP5 simulations. In particular, the serious lack of reflection of
10 solar radiation over the Southern Ocean in MRI-CGCM3 was drastically improved in MRI-ESM2. The score of the spatial
11 pattern of radiative fluxes at the top of the atmosphere for MRI-ESM2 is better than for any CMIP5 model. In this paper, we
12 set out comprehensively the various modifications related to clouds that contribute to the improved cloud representation, and
13 the main impacts on the climate of each modification. The modifications cover various schemes and processes including the
14 cloud scheme, turbulence scheme, cloud microphysics processes, interaction between cloud and convection schemes,
15 resolution issues, cloud radiation processes, interaction with the aerosol model, and numerics. In addition, the new
16 stratocumulus parameterization, which contributes considerably to increased low cloud cover and reduced radiation bias over
17 the Southern Ocean, and the improved cloud ice fall scheme, which alleviates the time-step dependency of cloud ice content,
18 are described in detail.

19

20 **1 Introduction**

21 Representation of clouds is crucially important for climate models because errors in simulated radiative fluxes are caused
22 mainly by poor representation of cloud rather than by errors in the clear sky radiation calculation. Consequently, biases in
23 clouds are the major factor for biases in the radiation budget and sea surface temperature ([SST](#)) that essentially determine the
24 basic performance of climate models. In addition, it is widely recognized that a large part of the uncertainty in projected
25 increases in surface temperature in global warming simulations by climate models arises from large uncertainties in cloud
26 feedback (e.g., Soden and Held, 2006; Soden et al., 2008). To obtain reliable cloud feedback in the climate models used for
27 the projection, clouds must be represented realistically, at least in their climatology. Therefore, cloud schemes and their related
28 processes are the most important atmospheric physical processes to be considered and carefully examined in the development
29 of climate models.

30 When a climate model undergoes a major upgrade with a new version name, many minor modifications are often included
31 rather than the introduction of a completely new sophisticated scheme. However, details are generally not provided of such
32 minor modifications including the technical information and the tuning of physics schemes related to clouds, although such
33 information is very useful and includes much scientific and technical value. Mauritsen et al. (2012) is one example of a
34 publication that provides practical and honest information for tuning of a climate model.

35 We participated in the fifth phase of the Coupled Model Intercomparison Project (CMIP5) (Taylor et al., 2012) and the
36 Cloud Feedback Model Intercomparison Project Phase 2 (CFMIP-2) (Bony et al., 2011) using our global climate model, MRI-
37 CGCM3 (Yukimoto et al., 2012, 2011). However, its representation of clouds was unsatisfactory. In the updated version of
38 our climate model, MRI-ESM2 (Yukimoto et al., 2019, ~~submitted~~), which is planned for use in CMIP6 (Eyring et al., 2015)
39 and CFMIP-3 (Webb et al., 2017) simulations, the representation of clouds is significantly improved. The score of the spatial
40 pattern of radiative fluxes for MRI-CGCM3 was worse than the average of the 48 CMIP5 models but the score for MRI-ESM2
41 is better than any of them. The improvement is particularly pronounced over the Southern Ocean. Trenberth and Fasullo (2010)
42 showed that a significant lack of clouds over the Southern Ocean is a serious problem in most climate models and causes huge
43 biases in shortwave radiative flux there. Although MRI-CGCM3 had this problem with biases that were worse than the average
44 CMIP5 model, the biases are dramatically reduced in the new model, MRI-ESM2.

45 The problems related to clouds in MRI-CGCM3 cover a broad range of issues. For instance, low cloud cover over the
46 mid-latitude and subtropical oceans is insufficient, the ratio of super-cooled liquid [water to cloud \(liquid and ice\)](#) water is too
47 small, the number concentration of cloud droplets of the Southern Ocean clouds is inadequate, the reflection of solar radiation
48 over the tropics is overestimated, vertical structures of low cloud transition are unrealistic, there are several coding bugs, and
49 ice water content shows strong time-step dependency. To solve these problems and give a better physical basis to the processes,
50 many modifications were implemented in MRI-ESM2. The model update includes:

- 51 (i) the introduction of a new stratocumulus parameterization,
- 52 (ii) a modified treatment of the Wegener–Bergeron–Findeisen (WBF) process,
- 53 (iii) a modified treatment of interaction between stratocumulus and shallow convection,
- 54 (iv) an increase in the vertical resolution,
- 55 (v) the introduction of a new cloud overlap scheme,
- 56 (vi) increased horizontal resolution for the radiation calculation,
- 57 (vii) various bug fixes,
- 58 (viii) updated aerosol size distributions,
- 59 (ix) an improved cloud ice fall scheme.

60 Item (i) is related to the cloud and turbulence schemes, (ii) to cloud microphysics process, (iii) to interaction between the cloud
61 and convection schemes, (iv) and (vi) to resolution issues, (v) to cloud radiation process, (viii) to the aerosol properties, and
62 (ix) to numerics. Improvements and modifications in this wide range of processes contribute to the improved cloud
63 representation in MRI-ESM2. It is worth describing the main effect of each modification separately with the background of

64 the modification, and such information is very useful for model developers. We would like to emphasize again that the
65 improvement of climate model performance due to updates is ordinarily contributed by the cumulative effect of a lot of
66 modifications, some of which may seem to be minor, rather than by the introduction of a new sophisticated scheme. In this
67 paper, the impacts of each modification are examined by comparing the result of a control AMIP simulation using the new
68 model MRI-ESM2 and results of AMIP experiments in which each updated process is separately turned off.

69 In addition, the new stratocumulus parameterization, which contributes considerably to increased low cloud cover and
70 reduced radiation bias over the Southern Ocean, includes scientifically new concepts, and the improved cloud ice fall scheme,
71 which alleviates the time-step dependency of cloud ice content, includes technically important issues. Therefore, these two
72 items are described in detail in the later section.

73
74

75 **2 Models and experiments**

76

77 **2.1 Models**

78 The cloud scheme in MRI-CGCM3 (Yukimoto et al., 2012, 2011; T_L159L48 in the standard configuration) is a two-
79 moment cloud scheme developed and modified from the Tiedtke cloud scheme (Tiedtke, 1993; Jakob 2000). Cloud fraction,
80 cloud liquid water and cloud ice water contents (LWC and IWC), number concentrations of cloud droplets and ice crystals are
81 prognostic variables. The source and sink terms of cloud fraction, LWC, and IWC are calculated basically following Tiedtke
82 (1993): the source terms include formation of stratiform cloud due to upward motion and temperature decrease and detrainment
83 from convection, and sink terms include evaporation. For the temperature range from -38 to 0 °C, deposition nucleation is
84 calculated based on Meyers et al. (1992), and depositional growth and evaporation for cloud ice are calculated following
85 Rutledge and Hobbs (1983). As processes for freezing of cloud droplets to ice crystals, immersion freezing and condensation
86 freezing (Bigg 1953; Murakami, 1990; Levkov et al., 1992; Lohmann, 2002), and contact freezing (Lohmann and Diehl, 2006;
87 Cotton et al., 1986) are calculated. Conversion of LWC to rain is calculated based on Manton and Cotton (1977) and Rotstayn
88 (2000). Melting of cloud ice and snow occurs just below an altitude where the atmospheric temperature is 273.15 K. In MRI-
89 ESM2 (Yukimoto et al. 2019, ~~submitted~~; T_L159L80 in the standard configuration), all these processes are essentially the same
90 as in MRI-CGCM3. The treatments of stratocumulus, the Bergeron–Findeisen effect, cloud ice fall, and conversion of IWC to
91 snow are discussed later in detail because they are modified from MRI-CGCM3 to MRI-ESM2.

92 Aerosols are calculated by the Model of Aerosol Species in the Global Atmosphere mark-2 revision 4-climate
93 (MASINGAR mk-2r4c) (Yukimoto et al., 2011; Tanaka et al., 2003; Yukimoto et al., 2019, ~~submitted~~), which is coupled to
94 MRI-ESM2. Five species of aerosols are utilized in the cloud and radiation schemes: sulfate, black carbon, organic matter, sea

95 salt (2 size modes), and mineral dust (6 size bins). The activation of aerosols into cloud droplets is calculated based on Abdul-
96 Razzak et al. (1998), Abdul-Razzak and Ghan (2000), and Takemura et al. (2005). The ice nucleation for cirrus clouds is
97 calculated using a parameterization of Kärcher et al. (2006), including homogeneous nucleation (Kärcher and Lohmann, 2002)
98 and heterogeneous nucleation (Kärcher and Lohmann, 2003).

99

100 2.2 Basic performance

101 First, we briefly show improvements from MRI-CGCM3 to MRI-ESM2 in the basic performance of the simulations.
102 Figure 1 shows the total cloud cover and its bias in the present-day climate from the historical simulations using MRI-CGCM3
103 and MRI-ESM2. Observational data for total cloud cover (Pincus et al., 2012; Zhang et al., 2012) that are derived from the
104 International Satellite Cloud Climatology Project (ISCCP; Rossow and Schiffer, 1999) D1 data and radiative flux observational
105 data from the Clouds and Earth's Radiant Energy Systems (CERES) Energy Balanced and Filled (EBAF; Loeb et al., 2009)
106 product are used as observational climatologies. It is clear that total cloud cover simulated by MRI-CGCM3 is much less than
107 the observations, especially over the Southern Ocean and subtropical oceans off the west coast of the continents. However,
108 total cloud cover is substantially increased in the simulation using MRI-ESM2 over these areas and the bias is reduced
109 significantly. As a result, a large negative bias in the upward shortwave radiative flux at the top of the atmosphere (TOA)
110 found in MRI-CGCM3 is reduced substantially in the simulation using MRI-ESM2. In addition, a positive bias in the tropics
111 is also reduced.

112 Figure 2 shows the Taylor diagrams (Taylor, 2001) for upward shortwave, longwave, and net radiative fluxes from the
113 48 CMIP5 models. The scores of spatial patterns of shortwave, longwave, and net radiative fluxes for MRI-CGCM3 are near
114 or worse than the average among the 48 CMIP5 models, but the scores for MRI-ESM2 are better than any of the models. The
115 scores for MRI-ESM2 are even almost comparable to the scores of the ensemble mean of CMIP5 models. Although the
116 uncertainty in the observational data for cloud radiative effect is larger than that of radiative fluxes at the top of the atmosphere,
117 the scores of cloud radiative effect for shortwave, longwave, and net radiation show similar characteristics to the corresponding
118 scores for TOA radiative fluxes (Fig. S1). This implies that improvement of TOA radiative fluxes in MRI-ESM2 can be
119 attributed to improvement of cloud representation in the model.

120

121 2.3 Experiments

122 The purpose of this paper is to identify the effect of each modification applied to the model under controlled conditions
123 in order to understand the significant improvement of the radiative flux in the new model. Therefore, we chose AMIP
124 simulations to avoid being influenced by changes in SST. A series of experiments with the new model MRI-ESM2 is performed,
125 with each modification summarized in Sect. 1 in turn set to the old (MRI-CGCM3) treatment. A list of sensitivity experiments

126 performed in the present study using MRI-ESM2 is given in Table 1. We ran the model from 2000 to 2010 and used the data
127 for 10 years from 2001 to 2010 for analysis.

128

129

130 **3 Updates and their impacts**

131 In this section, the updates from various aspects are explained with their backgrounds. The main impact of each update
132 is shown and discussed based on the comparison between the results of the updated new model and the experiments in which
133 each modification in turn is turned back to the old treatment.

134 **3.1 New stratocumulus parameterization**

135 Representation of low clouds including stratocumulus in climate models has been one of the most bothersome problems
136 for many years (e.g., Duynkerke and Teixeira, 2001; Siebesma et al., 2004), and low clouds are poorly reproduced even in the
137 state-of-the-art climate models (e.g., Nam et al., 2012; Su et al., 2013; Caldwell et al., 2013; Koshiro et al., 2018). As a result,
138 solar reflectance by clouds has significant negative biases over areas frequently covered by stratocumulus (e.g., Trenberth and
139 Fasullo, 2010; Li et al., 2013). A new stratocumulus scheme that utilizes a stability index that takes into account the effect of
140 cloud top entrainment (Kawai et al., 2017) was introduced instead of the old stratocumulus scheme (Kawai and Inoue, 2006).
141 A detailed description and physical interpretation are given in Sect. 4. Figure 3 shows that low cloud cover increases
142 significantly in the subtropical oceans off the west coast of the continents and over the Southern Ocean, which is a significant
143 result of upgrading the stratocumulus scheme. Low cloud cover is increased by more than 20% over the oceans off California,
144 Peru, Namibia, and west coast of Australia, and by more than 10% over the Southern Ocean. As a result, upward shortwave
145 radiative flux (reflection of solar insolation) also increases and this impact contributes to reducing the large bias in shortwave
146 radiative flux over these regions.

147

148 **3.2 Treatment of the WBF effect**

149 In recent years, several studies (e.g., McCoy et al., 2015; Cesana and Chepfer, 2013) revealed that ratios of super-cooled
150 liquid water with respect to cloud (liquid + ice) water in climate models are much lower than those in the Cloud–Aerosol Lidar
151 and Infrared Pathfinder Satellite Observations (CALIPSO; Winker et al., 2009) data (e.g., Hu et al., 2010; Cesana and Chepfer,
152 2013). Some studies pointed out that the lack of super-cooled liquid water in climate models is the source of insufficient solar
153 reflectance of clouds over the Southern Ocean (e.g., Bodas-Salcedo et al., 2016; Kay et al., 2016). Liquid clouds are optically
154 thicker than ice clouds if the cloud (liquid + ice) water content is the same, because the size of cloud droplets is much smaller
155 than that of ice crystals and this corresponds to larger number concentration for cloud droplets.

156 The WBF process is a deposition growth process of ice crystals at the expense of cloud droplets due to ice saturation
157 being lower than liquid water saturation. The WBF effect was treated in a way similar to Lohmann et al. (2007) in MRI-
158 CGCM3. When IWC is greater than a threshold of 0.5 mg kg^{-1} , all super-cooled water in the grid box is forced to evaporate
159 within the time step and all source terms for LWC are set to zero. However, this treatment caused excessive evaporation of
160 super-cooled water. In MRI-ESM2, when IWC exceeds the threshold, only the part of LWC that corresponds to the depositional
161 growth of ice crystals is evaporated within the time step. In addition, the source terms of LWC are not ignored but calculated
162 in a proper fashion. However, there is an arbitrariness about how these source terms are divided into the source terms of LWC
163 and IWC. The first reason for the arbitrariness is that the time step of our climate models is too long (30 minutes) to resolve
164 cloud microphysics and a part of the generated liquid water can change to ice crystals within this time step, especially when
165 IWC exceeds the threshold. The second reason is that the liquid water and ice water are assumed to be well mixed in the model
166 grid box if they coexist, as in most global climate models. However, there should be mixed phase parts, ice only parts, and
167 liquid only parts in a volume corresponding to the model grid box size (Tan and Storelvmo 2016). Therefore, it is difficult to
168 determine the LWC–IWC partitioning of the source terms theoretically. We decided to use a ratio derived by Hu et al. (2010)
169 based on satellite observations to determine the ratio of the source terms into LWC and IWC only when the WBF effect occurs,
170 that is, when IWC is greater than the threshold. This is an empirical and simple method, but this treatment can supplement the
171 defects of the modelled microphysics due to the uncertainty and complexity by utilizing observational data.

172 Figure 4 shows the ratio of super-cooled liquid water in clouds as a function of temperature in the simulations using new
173 and old treatments of the WBF effect. It is clear from the figure that the ratio of super-cooled liquid water is significantly
174 increased in the new treatment and close to the satellite observations of Hu et al. (2010); the ratio at 255 K is increased from
175 52% to 84% for the mass-weighted ratio and from 18% to 78% for the frequency ratio. Both mass-weighted ratio and frequency
176 ratio, which should correspond to the ratio derived from satellite observations, using the new treatment are close to the satellite
177 observations. [In MRI-ESM2, IWC production from the source terms of LWC based on partitioning using a function of Hu et](#)
178 [al. \(2010\) is dominant, and the contributions from a depositional growth and other freezing processes are considerably small.](#)
179 Figure 5 shows the impact of the new treatment of the WBF effect on TOA upward shortwave radiative flux. The reflection of
180 solar insolation is significantly increased over the Southern Ocean using the new treatment (Fig. 5), and consequently, this
181 new treatment contributes considerably to the reduction in shortwave radiation bias over the area shown in Fig. 1. The increase
182 in the ratio of super-cooled liquid water in MRI-ESM2 plausibly contributes to the higher climate sensitivity in the model than
183 in MRI-CGCM3, because an increased ratio of super-cooled liquid water weakens the cloud-phase feedback that negatively
184 contributes to cloud feedback (Tsushima et al., 2006; McCoy et al., 2015; Bodas-Salcedo et al., 2016; Kay et al., 2016; Tan et
185 al., 2016; Frey and Kay, 2018).

186 However, since the new treatment of the WBF effect is still rather simple, it cannot represent observed layered structures
187 with a thin super-cooled water layer at the top of cloud layers and ice layer below (Forbes and Ahlgrimm, 2014; Forbes et al.,
188 2016). In addition, it is possible that the curve of Hu et al. (2010) over-estimates the ratio of super-cooled liquid water (Cesana
189 and Chepfer, 2013; Cesana et al., 2016). [It should also be noted that empirical relationships including the ratio curve of Hu et](#)

190 [al. \(2010\)](#) may not hold completely in a future climate because a large number of meteorological factors contribute to form
191 [such relationships and they may change in a systematic way](#). Therefore, more sophisticated treatments need to be developed
192 in the future.

193

194 3.3 Interaction between stratocumulus and shallow convection

195 It is well-known that the altitude of the low-level cloud layer gradually increases westward in subtropical stratocumulus
196 regions, including off Peru, in association with the transition from stratocumulus to cumulus (Bretherton et al., 2010; Rahm
197 and Garreaud, 2010; Abel et al., 2010; Kawai et al., 2015). However, the vertical structures of the transition were unrealistically
198 discontinuous in the old model as seen in Fig. 6b. This discontinuity was caused by an unrealistically formed temperature
199 inversion just above the stratocumulus-like cloud layer due to excessive adiabatic heating by the convection scheme that
200 activates shallow convection in those regions. Therefore, in the new version, the occurrence of shallow convection is prevented
201 over the area where the conditions for stratocumulus occurrence (See Section 4.1 in more detail) are met. As a result, the
202 vertical structures of low-level clouds are significantly improved, as seen in Fig. 6a. Such a switch for shallow convection is
203 sometimes used in atmospheric models, although it is a simple and practical method. For example, a threshold of estimated
204 inversion strength (EIS; Wood and Bretherton, 2006) is used to determine the activation of shallow convection in version
205 CY43r3 of the European Centre for Medium-Range Weather Forecasts (ECMWF) Integrated Forecast System (IFS) (ECMWF,
206 2017).

207

208 3.4 Vertical resolution

209 The thickness of observed stratocumulus is typically 200–300 m (Wood 2012), but can be as thin as 50 m during the
210 daytime, especially in the Californian stratocumulus region (Betts, 1990; Duynkerke and Teixeira, 2001). The model vertical
211 resolution was increased from L48 (48 vertical levels) in the MRI-CGCM3 to L80 in the MRI-ESM2 (Yukimoto et al. 2019;
212 [submitted](#)), and the number of vertical layers in the atmospheric boundary layer was nearly doubled (from 5 to 10 layers below
213 900 hPa). As seen in Fig. 6c, the low cloud layer can be geometrically too thick in the model with resolution L48, which can
214 cause too high an albedo, because the vertical layer thickness is about 300 m at the level of 900 hPa and this is the minimum
215 thickness of clouds that can be represented in the model. Sensitivity of represented stratocumulus to model vertical resolution
216 has been widely reported (Teixeira, 1999; Bushell and Martin, 1999; Wang et al., 2004; Wilson et al., 2008; Neubauer et al.,
217 2014; Guo et al., 2015). Although several methods that compensate for insufficient vertical resolution have been developed,
218 including the use of vertical sub-levels (Wilson et al. 2007) and the introduction of areal cloud fraction, which is different from
219 volume cloud fraction (Brooks et al., 2005), we decided for the moment not to introduce those methods for simplicity and
220 consistency in the model physics.

221

222 3.5 Cloud overlap

223 In the longwave radiation scheme, maximum-random overlap (Geleyn and Hollingsworth, 1979) is adopted as a cloud
224 overlap assumption. In contrast, in the shortwave radiation scheme, total cloud cover in a column (the cloudy area) is first
225 calculated based on maximum-random overlap, and second, random overlap is adopted indirectly to calculate multiple
226 scattering in the cloudy area in the MRI-CGCM3 (Yukimoto et al., 2011, 2012). However, the inadequate treatment of the
227 cloud overlap assumption in the shortwave radiation scheme causes overestimation of the reflection of incident solar radiative
228 flux, especially for tower-shaped cumulus clouds with optically thin high-level clouds (e.g. anvil) (Nagasawa, 2012). In MRI-
229 ESM2, because a practical independent column approximation (PICA; Nagasawa, 2012) based on Collins (2001) was
230 implemented, the maximum-random overlap became available in the shortwave radiation scheme. Application of the
231 maximum-random overlap in the shortwave radiation scheme significantly decreased the reflection of shortwave radiative flux
232 over the tropical convection areas without varying total cloud cover (Fig. 7). This reduction makes a significant contribution
233 to reduce the excessive reflection of incident shortwave radiative flux over the tropics (see Fig. 1).

234

235 3.6 Horizontal resolution for radiation calculation

236 The computational cost for radiation calculation is heavy in climate models and this cost was reduced in MRI-CGCM3
237 by reducing the radiation calculation spatially and temporally. Full radiation computations were performed for every two grid
238 boxes in the zonal direction, and shortwave and longwave radiation was calculated 1-hourly and 3-hourly, respectively. Figure
239 8 shows the impacts of increased horizontal resolution for the radiation calculation (calculation for every single grid) (Fig. 8a,
240 8b) and increased frequency of calculation (1-hourly calculation) for longwave radiation (Fig. 8c, 8d). In both cases, low-level
241 clouds in the subtropics off the west coasts of the continents and at mid-latitudes increased, increasing shortwave reflectance
242 a little. This increase in low cloud cover can be attributed to improved cloud–radiation interactions: cloud-top longwave
243 cooling of low clouds, which is the primary physical process to maintain low clouds (e.g., Wood 2012), is consistently
244 calculated at the top of existing low clouds without spatial smoothing and temporal inconsistency. Either modification is
245 physically appropriate and improves the representation of low clouds. However, the total computational cost was increased by
246 5% for the spatial resolution modification and by 10% for the temporal resolution modification. Considering cost and merit
247 comprehensively, we decided to adopt the modification only for the spatial resolution and keep the temporal treatment
248 unchanged.

249

250 3.7 Bug fixes

251 No climate models are free from coding bugs, and they sometimes exert significant impacts on model results, although
252 they are rarely documented in publications. MRI-CGCM3 also had some bugs that affect the simulation results to some extent.

253 One of them is associated with the prognostic equations for number concentrations of the cloud particles. This bug caused a
254 problem of large number concentrations of cloud particles leading to excessive optical thickness and accompanying excessive
255 reflection of solar radiation, particularly for stratocumulus and stratus over the subtropics and northern Pacific region
256 (Tsushima et al., 2016). In addition, the bug caused a large decrease in the number concentration of cloud droplets and large
257 positive cloud feedback for such clouds in warmer climate simulations (Kawai et al. 2015). Several bugs including this serious
258 bug were fixed in MRI-ESM2.
259

260 **3.8 Aerosol size distributions**

261 Our climate models calculate number concentrations of aerosols from the mass concentrations using the prescribed
262 aerosol size distributions, and the number concentrations are used to calculate number concentrations of cloud particles.
263 Therefore, an appropriate treatment of the aerosol size distributions is important to estimate the aerosol effect on clouds.
264 Aerosol size distributions, namely the geometric mean radius and standard deviation in lognormal size distribution, were
265 modified in MRI-ESM2 based on recent observations. For example, the increase in the geometric mean radius of organic
266 carbon from 0.0212 (Chin et al., 2002) to 0.1 μm (Seinfeld and Pandis, 2006; Liu et al., 2012) in MRI-ESM2 causes a
267 significant decrease in the number concentration of cloud particles that originate from organic carbon. This modification
268 significantly decreases the response of cloud optical thickness to assumed changes in the emission of organic carbon. On the
269 other hand, the mode radius of fine mode sea salt is decreased from 0.228 (Chin et al., 2002) to 0.13 μm (Seinfeld and Pandis,
270 2006) and the change causes higher number concentration of cloud droplets originating from sea salt. In addition, the number
271 concentration of cloud condensation nuclei (CCN) originating from fine mode sea salt is multiplied by a factor of 2.0 after the
272 calculation from the number concentration of sea salt. This treatment is introduced because we use only two size modes (i.e.,
273 fine accumulation and coarse modes) of sea salt and the model cannot represent sea salt in the Aitken mode, although a part
274 of the sea salt in Aitken mode can work as CCN. Actually, the number concentration of sea salt in Aitken mode is difficult to
275 estimate from the mass concentration of aerosols because they contribute substantially to the number but contribute little to
276 the mass. To represent the contribution of sea salt in Aitken mode to CCN in a simple way, the factor of 2.0 is multiplied as a
277 provisional solution until sea salt in Aitken mode can be calculated explicitly. This factor is estimated from observational
278 studies (e.g., Covert et al., 1996; Clarke et al., 2006). In fact, a lower limit of the number concentration of cloud droplets has
279 been used in a significant number of state-of-the-art climate models to prevent too small number concentrations of cloud
280 droplets in clean air conditions (Hoose et al., 2009; Jones et al., 2001; Lohmann et al., 2007; Takemura et al., 2005). However,
281 it is pointed out that this lower limit drastically controls the magnitude of the aerosol indirect effect, for instance, measured as
282 the difference between present-day and preindustrial climates (Hoose et al., 2009). Therefore, the lower limit of cloud droplets
283 is not introduced in our model. We believe that our treatment is better than introducing a lower limit of cloud droplets although
284 it is quite simple, because the treatment has a more physical basis. This treatment increases cloud droplet number concentration
285 by more than 30% and also increases reflection of shortwave radiation by 4 W m^{-2} over the Southern Ocean (Fig. 9).

286

287 **3.9 Ice sedimentation and ice conversion to snow**

288 The method for calculating cloud ice sedimentation in the MRI-CGCM3 was not sophisticated, and it caused unrealistic
289 ice sedimentation and strong time-step dependency of IWC. While IWC is a prognostic variable in the MRI-CGCM3, snow is
290 not but it is treated as snow flux in the model. A part of IWC is diagnosed as snow and removed from the IWC at each time
291 step and falls down to the surface within one time step. The main problem was that the ratio of snow was not proportional to
292 the time step. As a result, a substantial amount of snow is repeatedly removed from IWC when the time step is shortened. To
293 solve the problem, the treatment of cloud ice sedimentation and conversion of cloud ice to snow was improved based on the
294 study of Kawai (2005). Figure 10 shows that IWC is large for a time step of 3600 s but monotonically decreases with shorter
295 time steps. On the other hand, IWC is not affected by the time step in the control simulation that uses the modified scheme of
296 ice sedimentation and ice conversion to snow. A detailed description of the modification is given in Sect. 4, because this
297 modification contains some important insights and solutions related to the numerical issues.

298

299 **3.10 Summary of impacts on shortwave radiative flux**

300 Figure 11 summarizes the impacts of each modification on zonal means of low cloud cover and TOA upward shortwave
301 radiative flux. The new stratocumulus scheme contributes to an increase in low cloud cover mainly over the Southern Ocean,
302 and the suppression of shallow convection under stratocumulus conditions contributes a low cloud cover increase over the
303 mid-latitudes in the Southern Hemisphere. Increased horizontal resolution in the radiation calculation additionally contributes
304 to the low cloud cover increase. The increase in reflection of solar radiation over the Southern Ocean and mid-latitudes in the
305 Southern Hemisphere is largely contributed by the new stratocumulus scheme, the new treatment of the WBF effect (especially
306 around 60°S), the doubled number concentration of sea salt CCN, and the treatment of shallow convection suppressed under
307 stratocumulus conditions (over latitudes lower than the areas impacted by other modifications). The new treatment of the WBF
308 effect and doubled number concentration of sea salt CCN increase the reflection of solar radiation by increasing cloud optical
309 thickness. A new cloud overlap scheme, PICA, contributes to reduction in solar radiation reflection over the tropics without
310 changing the cloud cover. These modifications in MRI-ESM2 significantly reduce the large bias in the solar radiation reflection
311 present in MRI-CGCM3, which is negative over the Southern Ocean and positive over the tropics (Fig. 1e, 1f, and Fig. 11c).
312 Note that the significant improvement in the shortwave radiative flux is not attributed to the introduction of a new advanced
313 scheme but to the cumulative effect of many minor modifications.

314

315 **3.11 Comments on tuning**

316 At the end of this section, we give a brief description of the model tuning related to clouds. At a stage of developing
317 schemes, a number of amip type simulations (with typical one-year length) were performed using atmospheric and aerosol
318 coupled model, to check the basic behavior of schemes and the basic impacts on radiative fluxes. At a tuning stage, five-year
319 runs of amip type simulations were mainly examined. The main targets for tuning parameters related to clouds in MRI-ESM2
320 were global-mean biases and root-mean square errors of shortwave and longwave radiative fluxes at the top of the atmosphere.
321 The tuning parameters related to clouds are parameters which affect differently by cloud types and control cloud properties
322 such as cloud cover, cloud water content, and cloud number concentration. In the stratocumulus parameterization (Section 3.1),
323 the threshold value of ECTEI was tuned to increase Southern Ocean clouds as described in Section 4.1.3. The relatively large
324 mode radius of sulfate of 0.10 μm (possible range: 0.05 – 0.10 μm) was chosen to obtain smaller cloud droplet number
325 concentration to prevent an excessive aerosol-cloud interaction. Treatment of the WBF effect (Section 3.2), cloud overlap
326 scheme (Section 3.5), schemes for ice sedimentation and ice conversion to snow (Section 3.9), and others (Sections 3.3, 3.4,
327 3.6, and 3.7) were not tuned. Descriptions of the model tuning (other than cloud-related parameters) are given in Yukimoto et
328 al. (2019).

330 **4 Detailed description of schemes**

331 In this section, modifications and improvements in two schemes are explained in detail, because they include scientifically
332 new concepts and technically important insights and solutions related to the numerical issues; one is the new stratocumulus
333 parameterization and the other is the improved cloud ice fall scheme.

334 **4.1 New stratocumulus parameterization**

335 **4.1.1 Old parameterization and problems**

336 In the MRI-CGCM3, a stratocumulus scheme slightly modified from Kawai and Inoue (2006), originally developed from
337 Slingo (1980, 1987), was used to represent subtropical stratocumulus. In that scheme, stratocumulus is formed when the
338 following four conditions are met: (i) there is a strong inversion above the model layer, (ii) the layer near the surface is not
339 stable (to guarantee existence of a mixed layer), (iii) the model layer height is below the level of 940 hPa, and (iv) the relative
340 humidity of the model layer exceeds 80%. When all of these conditions are met, cloud cover is determined as a function of the
341 inversion strength, in-cloud cloud water content is determined to be proportional to the saturation specific humidity, and the
342 vertical mixing at the top of the cloud layer is reduced to approximately zero to prevent excess cloud top entrainment.

343 Although this scheme can reproduce subtropical stratocumulus and the cloud radiative effect relatively well, it has several
344 problems. First, it does not give enough low clouds over mid-latitude oceans, especially the Southern Ocean. Low clouds off

345 the west coast of the continents, including off California, off Peru, and off Namibia, are also insufficient, especially areas far
 346 from the coast. The second problem is related to the use of inversion strength in parameterization in climate models, which is
 347 calculated from the difference of potential temperature between two adjacent vertical model layers. Climate models cannot
 348 reproduce realistic strong inversions because their vertical resolution is totally insufficient. Furthermore, the inversion strength
 349 reproduced in climate models strongly depends on the model vertical resolution. Therefore, the parameter has to be tuned for
 350 each model, if the inversion strength is directly utilized in the parameterization. In addition, there is a strong positive feedback
 351 between cloud fraction of low cloud and the inversion strength at the top of the cloud. The positive feedback makes it difficult
 352 to utilize inversion strength in the parameterization of low cloud fraction. The third problem is that the vertical structure with
 353 a smooth transition from stratocumulus to cumulus cannot be reproduced because the parameterization is limited to below the
 354 level of 940 hPa (see Kawai and Inoue, 2006). To solve these problems, we decided to utilize a criterion that represents the
 355 structure of the lower troposphere as a whole (“non-local”) rather than a detailed local vertical structure.

356 4.1.2 New index for low cloud cover

357 Estimated inversion strength (EIS; Wood and Bretherton, 2006), which is a modification of lower tropospheric stability
 358 (LTS; Klein and Hartmann 1993), is an index that correlates well with low cloud cover and has been used in many studies.
 359 However, EIS takes into account only the temperature profile and does not include information on water vapour. Kawai et al.
 360 (2017) developed an index for low cloud cover, the estimated cloud-top entrainment index (ECTEI). This index is deduced
 361 from a criterion of cloud top entrainment (Randall, 1980; Deardorff, 1980; Kuo and Schubert, 1988; Betts and Boers, 1990;
 362 MacVean and Mason, 1990; MacVean, 1993; Yamaguchi and Randall, 2008; Lock, 2009) and includes information on both
 363 the vertical profile of temperature and that of water vapour. The definition of ECTEI is as follows:

$$364 \text{ECTEI} \equiv \text{EIS} - \beta L / c_p (q_{\text{surf}} - q_{700})$$

365 where L is latent heat, c_p is the specific heat at constant pressure, q_{surf} and q_{700} are the specific humidity at the surface and 700
 366 hPa, respectively, $\beta = (1 - k) C_{\text{qgap}}$, C_{qgap} is a coefficient ($= 0.76$), and k is a constant ($= 0.70$; MacVean and Mason 1990).

367 Figure 12 shows the climatologies of low stratiform cloud cover and the stability indexes, LTS, EIS, and ECTEI, for
 368 December to February and June to August. Cloud cover data were obtained from shipboard observations, the extended edited
 369 cloud report archive (EECRA; Hahn and Warren, 2009), and stability indexes were calculated using the ECMWF 40-year Re-
 370 Analysis (ERA-40) data (Uppala et al., 2005) for 1957–2002. The definition of low cloud cover (LCC) in the observations is
 371 the combined cloud cover of stratocumulus, stratus, and sky-obscuring fog, which is the same conventional definition as
 372 employed in Klein and Hartmann (1993) and Wood and Bretherton (2006). When LCC and LTS maps are compared, the
 373 contrast between the subtropics and mid-latitudes is different. LTS is weighted more over the subtropics than over mid-latitudes
 374 while LCC is dominant over mid-latitudes. In EIS maps, the value is more weighted in mid-latitudes than in the subtropics,
 375 compared with LTS, and the EIS geographical patterns are closer to LCC patterns than LTS patterns, as it is well-known that
 376 EIS corresponds to LCC better than LTS. In ECTEI maps, the weight is even larger in mid-latitudes than for EIS and the
 377 ECTEI geographical patterns are even closer to LCC patterns than the EIS patterns. These characteristics suggest that EIS does

378 not adequately represent the large occurrence of low cloud over cold oceans including the Southern Ocean and ECTEI can be
379 more appropriate for representation of LCC. Figure 13 shows the relationships between the LCC and the stability indexes,
380 LTS, EIS, and ECTEI. It shows that ECTEI has the best correlation with LCC with correlation coefficients $R = 0.23$ for LTS,
381 $R = 0.83$ for EIS, and $R = 0.90$ for ECTEI.

382 4.1.3 New parameterization and improvements

383 In our new scheme, the relationship between ECTEI and LCC is not directly used but ECTEI is used as a threshold of a
384 treatment in the turbulence scheme. In our climate models, vertical smoothing of vertical diffusivity is employed to represent
385 simply the mixing effect due to cloud top entrainment and part of the mixing due to shallow convection. In MRI-ESM2, if
386 ECTEI is larger than a threshold value, the smoothing is prevented, which means the turbulence at the top of the boundary
387 layer is suppressed, and the lower limit of vertical diffusivity is set to a much smaller value (virtually zero) than the original
388 one. This means that cloud top entrainment in the model is switched on and off depending on an ECTEI threshold. In the
389 original setting, the threshold value was set to 0 K and the condition of not stable near-surface layer (to guarantee existence of
390 a mixed layer) was imposed (Kawai 2013). However, after model tuning, the threshold value of ECTEI was set to -2.0 K;
391 (possible range: $-3.0 - +3.0$ K), and the condition of mixed layer existence was removed to apply the suppression of cloud top
392 mixing not only to stratocumulus conditions but also to advection fog conditions, where the near-surface layer is stable. The
393 introduction of this scheme has led to an increase in low cloud cover, especially over the mid-latitude ocean, including the
394 Southern Ocean, and the radiation bias is significantly reduced (Fig. 3).

395 The application of a condition that represents the detailed local vertical structure may appear to be more physically based
396 than a "non-local" condition. However, parameterizations based on local vertical structures are not appropriate in some cases
397 where (i) model resolution is not sufficient to represent the detailed physical process or (ii) the feedback between the parameters
398 and the variables that should be obtained is very strong. In such cases, the parameters that represent the whole structure of the
399 lower troposphere can produce more robust and reasonable results, although empirical relations are required to construct "non-
400 local" parameterizations.

401 4.1.4 Brief discussion on climate change simulations

402 It is well-known that changes in LCC in warmer climates cannot be explained by changes in LTS (e.g., Williams et al.,
403 2006; Medeiros et al., 2008; Lauer et al., 2010). The mechanism of this discrepancy is also well-understood: inevitable decrease
404 of moist adiabatic lapse rate in the free atmosphere in warmer climates causes increase in LTS (e.g., Miller, 1997; Larson et
405 al., 1999), even though the inversion strength that probably contributes to determine LCC does not change (e.g., Wood and
406 Bretherton, 2006; Caldwell and Bretherton, 2009). It was expected that an index EIS could avoid this problem and could be
407 used for discussion of LCC changes under warmer climates because EIS is a more physics-based index that represents inversion
408 strength at the cloud top more directly. However, more recently, it turned out that LCC tends to decrease, although EIS
409 increases in warmer climates in most climate models (e.g., Webb et al., 2013). Subsequently, it was shown by Qu et al. (2014)

410 that changes (including variations in the present climate and future changes) in LCC can be determined by a linear combination
411 of changes in EIS (positive correlation) and SST (negative correlation). Kawai et al. (2017) derived the linear combination
412 from the index ECTEI and showed that a decrease in LCC under increased EIS in warmer climates can be explained based on
413 the ECTEI change (see Kawai et al. (2017) for more detail). It is true that a usage of empirical relationships obtained in the
414 present climate for climate change simulations has a possibility of causing spurious climate feedback. On the other hand, we
415 would like to note that ECTEI is even more physics-based index than EIS, the relationship is not used directly for cloud
416 formation but used as a threshold for cloud top mixing, and ECTEI can explain positive low cloud feedback, although the risk
417 of spurious climate feedback still cannot be eliminated.

418

419 4.2 Ice sedimentation and ice conversion to snow

420 4.2.1 Old treatment and problems

421 Treatment of ice sedimentation in climate models is awkward because the product of the terminal velocity of cloud ice
422 v_{ice} (typical value $\sim 0.5 \text{ m s}^{-1}$) and the time step Δt (for example, 1800 s in MRI-CGCM3 and MRI-ESM2) can exceed the
423 thickness of the vertical layer Δz ($\sim 500 \text{ m}$) in climate models. In such cases the explicit calculation is invalid and numerical
424 instability may occur because a vertical Courant–Friedrichs–Lewy (CFL) condition is violated. To avoid this problem, various
425 measures have been taken. Rotstayn (1997) reviewed the following four treatments: (A) to set an artificial limit to the
426 sedimentation flux for preventing defective calculation; (B) to adopt a 'fall-through' assumption; (C) to use an implicit scheme;
427 and (D) to use an analytically integrated scheme. Discussing the problems associated with each treatment, he concluded that
428 the last one (D) was the most suitable. Although adopting shorter time steps for selected processes that is called substepping
429 (e.g., Morrison and Gettelman, 2008) would be an ideal solution, it can increase computational cost to some degree.

430 In MRI-CGCM3, IWC was divided into ice crystals and snow using a size threshold of $100 \mu\text{m}$. The size distribution of
431 ice particles is assumed to follow a Marshall–Palmer distribution as described in Rotstayn (1997):

$$432 P_i(D_i) = \lambda_i e^{-\lambda_i D_i}$$

433 where D_i (m) is the diameter of ice particles, λ_i (m^{-1}) is the slope factor, and the distribution $P_i(D_i)$ is normalized to 1. The
434 slope factor can be written as follows:

$$435 \lambda_i = \left(\frac{\pi \rho_i N_i}{\rho_a q_i} \right)^{1/3}$$

436 where ρ_i (kg m^{-3}) is the density of ice, N_i (m^{-3}) is the number concentration of ice crystals, ρ_a (kg m^{-3}) is air density, and q_i (kg
437 kg^{-1}) is IWC. The ratios of cloud ice crystals with size less than $100 \mu\text{m}$ with respect to total ice crystals can be obtained
438 analytically by integrating the probability density function as follows:

$$439 r_{iw} = 1 - \frac{1}{6} \{ (\lambda_i D_{100})^3 + 3(\lambda_i D_{100})^2 + 6(\lambda_i D_{100}) + 6 \} e^{-\lambda_i D_{100}}$$

440
$$r_{in} = 1 - e^{-\lambda_i D_{100}}$$

441 where D_{100} (m) is particle size of 1×10^{-4} (m) ($\approx 100 \mu\text{m}$), and r_{iw} and r_m are ratios of cloud ice crystals for mass and number
 442 concentrations. A sedimentation velocity (m s^{-1}) is calculated based on Heymsfield (1977), Heymsfield and Donner (1990),
 443 and Rotstayn (1997):

444
$$v_{ice} = 3.23 \left(\frac{\rho_a q_i r_{iw}}{a} \right)^{0.17} \quad (1)$$

445 where a is cloud fraction. Ice crystals of $r_{iw} q_i$ fall with sedimentation velocity v_{ice} , and snow mass $(1 - r_{iw}) q_i$ is assumed to
 446 fall down to the surface within a time step. Removal of the snow part based on this kind of diagnostic partition is used in some
 447 cloud schemes. In version CY25r1 of the ECMWF IFS (ECMWF, 2002), IWC is divided into two categories with sizes larger
 448 and smaller than $100 \mu\text{m}$ following a function in McFarquhar and Heymsfield (1997; hereafter, MH97) and the larger size
 449 portion of IWC is considered to fall through to the ground within a time step. In MRI-CGCM3, the equation of IWC to be
 450 solved is as follows:

451
$$\frac{\partial q_i}{\partial t} = C_g + \frac{\partial}{\partial z} (v_{ice} \rho_a r_{iw} q_i) - \frac{R_i}{\rho_a \Delta z} - \frac{v_{ice}}{\Delta z} r_{iw} q_i - \frac{(1-r_{iw})q_i}{\Delta t} \quad (2)$$

452 where C_g ($\text{kg kg}^{-1} \text{s}^{-1}$) is the generation rate of IWC, R_i ($\text{kg m}^{-2} \text{s}^{-1}$) is the ice sedimentation flux into the layer from above, Δz
 453 (m) is the layer thickness, and Δt (s) is the model time step. The second and the third terms on the right-hand side correspond
 454 to the ice sedimentation calculation (e.g., Smith, 1990; Rotstayn, 1997). An analytically integrated solution (Rotstayn, 1997;
 455 ECMWF, 2002) was used to obtain IWC after one time step.

456 However, this treatment contains some problems. The first is that a part of cloud ice larger than $100 \mu\text{m}$ is eliminated
 457 from the atmosphere repeatedly when a short time step is used, because the shape of the size distribution and the ratio of ice
 458 portions larger than and smaller than $100 \mu\text{m}$ is insensitive to IWC change. This causes strong time-step dependency of IWC:
 459 IWC monotonically decreases with shorter time steps from 3600 s to 300 s as seen in Fig. 10. The second problem is that the
 460 sedimentation velocity calculated from Eq. (1) is too large for ice with size smaller than $100 \mu\text{m}$. This is because the
 461 sedimentation velocity is supposed to represent a weighted value for the whole ice content that includes all sizes of ice, and
 462 sedimentation velocity varies widely with particle size.

463 4.2.2 New scheme and improvements

464 Considering the wide range of sedimentation velocity, the velocities of falling cloud ice representing both small and large
 465 particles are derived separately (originally reported in a preliminary report, Kawai, 2005). Observed size-distribution functions
 466 of cloud ice of MH97 and size-velocity relationships for cloud ice (Heymsfield and Iaquinta 2000) were integrated over size
 467 using a procedure similar to Zurovac-Jevtić and Zhang (2003). See Supplement A for the detailed derivation. While they
 468 derived only one velocity representing the total cloud ice, two velocities are derived in this study for a more sophisticated
 469 treatment of sedimentation. The ice-fall velocity for particles smaller [larger] than $100 \mu\text{m}$, v_i [v_s] (m s^{-1}), is obtained as a

470 function of ice water content smaller [larger] than 100 μm , $\text{IWC}_{<100}$ [$\text{IWC}_{>100}$] (kg m^{-3}), as below (note that the unit is not (kg
 471 kg^{-1}) but (kg m^{-3}):

$$472 \quad v_i = 1.56(\text{IWC}_{<100})^{0.24} \quad (3)$$

$$473 \quad v_s = 2.23(\text{IWC}_{>100})^{0.074} \quad (4)$$

474 Figure 14 shows the velocities v_i and v_s . The velocity of cloud ice smaller than 100 μm is much smaller than the
 475 conventionally used velocity of ice of Rotstain (1997). Therefore, it is inappropriate to represent the velocity of ice with size
 476 smaller than 100 μm using the velocity of Eq. (1), and Eq. (3) is more appropriate for calculating the velocity. The figure also
 477 shows that cloud ice larger than 100 μm has a velocity of about 1 m s^{-1} . Therefore, the sedimentation cannot be calculated
 478 appropriately with the time step used in our climate models, and the treatment of instant fall of snow (large ice) through to the
 479 surface is unavoidable, unless substepping is introduced.

480 In MRI-CGCM3, it was assumed that the ratio of snow calculated from the Marshall–Palmer distribution can be applied
 481 anytime and anywhere without taking account of the history of the cloud processes. In this case, conversion of ice crystal into
 482 snow is not proportional to model time step and it causes the strong time-step dependency of IWC. If a conversion rate of ice
 483 crystals into snow is available, we can avoid this time-step dependency. To obtain the rate, we assume that the ratio given by
 484 MH97 may be regarded as a ratio between ice crystals and accumulated snow from the layers above, which is converted from
 485 ice crystals at a certain rate. In this concept, the ratio of snow should increase as the depth from the cloud top increases. In the
 486 derivation of the rate C_{12S} ($\text{kg kg}^{-1} \text{s}^{-1}$), simple assumptions were introduced: (a) the concentration of cloud ice is vertically
 487 homogeneous, (b) produced snow concentration is accumulated downward, (c) the observation depth of the ratio is H_c (m)
 488 from the top of a cloud. Under these assumptions, the rate can be obtained as follows (see Appendix A for the derivation):

$$489 \quad C_{12S} = \frac{1-\alpha_i}{\alpha_i} \frac{v_s}{H_c} q_i \quad (5)$$

490 where α_i is the ratio of cloud ice content with particle sizes smaller than 100 μm to the total cloud ice content (see Supplement
 491 A.2 for details: Fig. S2 shows α_i and the equation is Eq. (S10)). In this study, $H_c = 2,000$ m is assumed in reference to MH97.
 492 The equation of IWC to be solved is as follows:

$$493 \quad \frac{\partial q_i}{\partial t} = C_g + \frac{\pm}{\rho_w \Delta z} (v_i \rho_w q_i) \frac{R_i}{\rho_a \Delta z} - \frac{v_i}{\Delta z} q_i - D_{12S} q_i \quad (6)$$

494 where $D_{12S} = C_{12S}/q_i$, where $D_{12S} = C_{12S}/q_i$. Note that although the ratio α_i obtained from Eq. (S10) is used to calculate the
 495 conversion rate C_{12S} , it is not used to directly determine the ratio between small ice crystals and snow differently from in Eq.
 496 (2). An analytically integrated solution is used to obtain IWC after one time step.

497 Figure 10 shows that IWC is not affected by time step in the control simulation that uses the modified scheme of ice
 498 sedimentation and ice conversion to snow, while the old scheme that was used in MRI-CGCM3 shows strong time-step
 499 dependency. The improvement can mainly be attributed to the fact that the conversion of ice to snow is proportional to the
 500 time step: the last term of the right-hand side in Eq. (6) does not explicitly depend on Δt , while the one in Eq. (2) does. In
 501 addition, the slower sedimentation velocity in the new formulation contributes to more reasonable calculation of ice crystal

書式を変更: 英語 (米国)

502 sedimentation because processes with short time-scales compared to the model time step may be unphysically calculated. In
503 many climate models, the terminal velocity of cloud ice has been represented by a single velocity whose typical value is ~ 0.5
504 m s^{-1} (e.g., Heymsfield, 1977; Heymsfield and Donner, 1990), and the whole cloud ice content in the grid box falls with that
505 velocity (e.g., Rotstayn, 1997; Smith, 1990). However, as is evident from Fig. 14, the velocity of ice crystals smaller than 100
506 μm is $\sim 0.1 \text{ m s}^{-1}$ and much smaller than the typical value representing all sizes ($\sim 1 \text{ m s}^{-1}$). Small size ice crystals should remain
507 in the air for longer. On the other hand, some models diagnose the removal of snow portion from the total IWC assuming a
508 fixed size distribution without taking the history of the cloud processes into account (e.g., ECMWF, 2002). However, this
509 causes time-step dependency, as discussed above. Note also that size distribution must change depending on the distance from
510 the cloud top, although such dependence is not taken into account explicitly in most studies or treatments in climate models.
511 We have clarified such problems and proposed a practical solution for them in the present paper.

512
513

514 **5 Summary**

515 In the development of the climate model MRI-ESM2 that is planned for use in CMIP6 and CFMIP-3 simulations, the
516 representations of clouds are significantly improved from the previous version MRI-CGCM3 used in CMIP5 and CFMIP-2
517 simulations. The score of the spatial pattern of radiative fluxes at the top of the atmosphere for MRI-ESM2 is better than any
518 of the 48 CMIP5 models. In this paper, we presented comprehensively various modifications related to clouds, which
519 contribute to the improved cloud representation, and their main impacts. The modifications cover various schemes and
520 processes including the cloud scheme, turbulence scheme, cloud microphysics processes, the interaction between cloud and
521 convection schemes, resolution issues, cloud radiation processes, the aerosol properties, and numerics. Note that the
522 improvement of performance in climate models due to an update is ordinarily contributed by the cumulative effect of many
523 minor modifications rather than by the introduction of a new advanced scheme. In addition, the new stratocumulus
524 parameterization and improved cloud ice fall scheme are described in detail, because they include scientifically new concepts
525 and technically important issues. As a result, this paper will be useful for model developers and users of our CMIP6 outputs,
526 especially those related to clouds.

527 The most remarkable improvement addressed the serious lack of upward shortwave radiative flux over the Southern
528 Ocean in the old version. This improvement was obtained mainly by (i) an increase in low cloud cover due to the
529 implementation of the new stratocumulus scheme, a new treatment of the suppression of shallow convection under
530 stratocumulus conditions, and increased horizontal resolution for the radiation calculation, (ii) an increase in the ratio of super-
531 cooled liquid water due to the modified treatment of the WBF effect, and (iii) an increase in cloud droplet number concentration
532 by taking the effect of small size sea-salt aerosols into account. Items (ii) and (iii) contribute to an increase in the optical
533 thickness of clouds. The excessive reflection of solar radiation over the tropics in MRI-CGCM3 was substantially reduced by

534 the introduction of a new cloud overlap scheme, PICA. Increased vertical resolution from L48 to L80 and a treatment of the
535 suppression of shallow convection under stratocumulus conditions contribute to improve the vertical structure of the transition
536 from subtropical stratocumulus to cumulus. In addition, improved treatments of cloud ice sedimentation and conversion of
537 cloud ice to snow, which are based on more accurate physics than the old ones, alleviated the strong time-step dependency of
538 IWC.

539 However, the modifications in MRI-ESM2 are still relatively simple and ad hoc in some cases. Therefore, we should
540 continue to develop various schemes and processes related to clouds, especially cloud microphysics and the treatment of cloud
541 inhomogeneity within a model grid box, by introducing more sophisticated concepts.

542 On a final note, we acknowledge the many evaluation and intercomparison studies related to clouds for CMIP multi-
543 models, which have given us useful information for model development (e.g., Jiang et al. (2012) for vertical profiles of cloud
544 water content and water vapour; [Lauer and Hamilton \(2013\) for liquid water path](#); Su et al. (2013) for vertical profiles of cloud
545 fraction and cloud water content under different large-scale environments; McCoy et al. (2015) and Cesana et al. (2015) for
546 ratios of super-cooled liquid water and ice; Nam et al. (2012) for cloud radiative effect and vertical structure of low clouds;
547 Nuijens et al. (2015) for vertical structures and temporal variations of trade-wind cumulus; Bodas-Salcedo et al. (2014) for
548 cloud and radiation biases over the Southern Ocean; Kawai et al. (2018) for marine fog; Suzuki et al. (2015) for warm rain
549 formation process; Tsushima et al. (2013) for occurrence frequency and cloud radiative effect of each cloud regime). It is
550 impossible for a modeller to examine all of these characteristics in their own model, because there are many aspects to examine
551 even for cloud related values alone and these evaluations need specific knowledge and careful treatment. Therefore, these
552 evaluation activities are very helpful for modellers to improve and develop their models.

553
554

555 **Code and Data availability**

556 Access to the simulation data can be granted upon request. The MRI-ESM2 code is the property of MRI/JMA and not
557 available to the general public. Access to the code can be granted upon request, under a collaborative framework between MRI
558 and related institutes or universities. The code can be provided to the editor and the reviewers for the purpose of the review of
559 the manuscript.

560
561

562 **Appendix**

563 **A. Derivation of the conversion rate of cloud ice crystals to snow**

564 The conversion rate of cloud ice crystals to snow (cloud ice particles whose size is larger than 100 μm are called “snow”
565 here) in the new treatment is derived under the simple assumptions described below. Although these assumptions are rather
566 rough, the advantage is that this rate utilized in the scheme is derived from observational relationships for tropical cirrus.

567 It is assumed that the ratio between cloud ice crystals and snow is not the same throughout a cloud, but depends on the
568 depth from the cloud top. It is presumed that the ratio of small cloud ice crystals is large near the cloud top and the ratio of
569 snow (large cloud ice) increases downward in the cloud, because upper cloud ice crystals are continuously converted to snow
570 and the density of snow, which falls with velocity much faster than cloud ice crystals, is accumulated downward. Therefore,
571 the ratios should be a function of the distance from the cloud top, and the ratios α_i in MH97 should be regarded as the ratio at
572 a certain distance from the cloud top.

573 To derive the conversion rate in this study, cloud ice content q_i (kg kg^{-1}) was assumed to be vertically homogeneous in
574 the cloud. The snow density (kg m^{-3}) that is produced by a unit volume of cloud ice crystals existing at upper altitude is C_{12S}
575 $\rho_a v_s^{-1}$, using a conversion rate of cloud ice to snow C_{12S} ($\text{kg kg}^{-1} \text{s}^{-1}$). Consequently, the snow density at height z can be written
576 as follows, using the cloud top height z_{ctop} .

577
$$\int_z^{z_{\text{ctop}}} C_{12S} \frac{\rho_a}{v_s} dz \approx \frac{z_{\text{ctop}} - z}{v_s} \rho_a C_{12S}$$

578 where a constant value is used for ρ_a regardless of the height for simplicity. Then snow content per unit air mass is $C_{12S} H_c v_s^{-1}$
579 (kg kg^{-1}) using $H_c \equiv z_{\text{ctop}} - z$. On the other hand, the ratio of cloud ice crystals to snow can be written as follows using the
580 observational function α_i by MH97:

581
$$q_i \frac{H_c}{v_s} C_{12S} = \alpha_i (1 - \alpha_i)$$

582 Therefore, C_{12S} can be derived as follows:

583
$$C_{12S} = \frac{1 - \alpha_i}{\alpha_i} \frac{v_s}{H_c} q_i$$

584
585

586 **Author contribution**

587 HK was responsible for most aspects of model developments related to the representation of clouds. SY performed tuning
588 of clouds simulated in MRI-ESM2 and many sensitivity tests. TK performed coding related to aerosol optical properties and
589 the output format of the model. NO and TT developed the aerosol model and contributed to the improvements of the aerosol
590 radiation and aerosol cloud interactions. RN developed PICA and HY implemented the scheme into MRI-ESM2. SY and TK
591 performed many model simulations, and TK and HY contributed to find coding problems in the original cloud scheme. All

592 authors contributed to related discussions. HK wrote the first draft of the article, and all authors contributed to the writing of
593 the final version of the article.

594

595 **Acknowledgements**

596 We acknowledge the editor for handling this paper and the two anonymous reviewers for their supportive and insightful
597 comments. Several datasets (Pincus et al., 2012; Zhang et al., 2012) used in this work were obtained from the obs4MIPs project
598 (<https://www.earthsystemcog.org/projects/obs4mips/>) hosted on the Earth System Grid Federation (<http://esgf.llnl.gov>). This
599 study was partly supported by “Integrated Research Program for Advancing Climate Models: TOUGOU” from the Ministry
600 of Education, Culture, Sports, Science and Technology (MEXT), Japan. Additionally, it was supported by the Japan Society
601 for the Promotion of Science (JSPS) KAKENHI Grant Numbers JP26701004, JP16H01772, JP18H05292, ~~and~~ JP18H03363,
602 ~~and~~ JP19K03977 and the Environment Research and Technology Development Fund (2-1703 and S-12) of the Environmental
603 Restoration and Conservation Agency, Japan. Kohei Yoshida made efforts to determine vertical model levels in MRI-ESM2,
604 and Eiki Shindo kindly supported HK to perform model experiments.

605

606 **References**

607

- 608 Abdul-Razzak, H. and Ghan, S. J.: A parameterization of aerosol activation: 2. Multiple aerosol types, *J. Geophys. Res.*,
609 105(D5), 6837, doi:10.1029/1999JD901161, 2000.
- 610 Abdul-Razzak, H., Ghan, S. J. and Rivera-Carpio, C.: A parameterization of aerosol activation: 1. Single aerosol type, *J.*
611 *Geophys. Res.*, 103(D6), 6123, doi:10.1029/97JD03735, 1998.
- 612 Abel, S. J., Walters, D. N. and Allen, G.: Evaluation of stratocumulus cloud prediction in the Met Office forecast model during
613 VOCALS-REx, *Atmos. Chem. Phys.*, 10(21), 10541–10559, doi:10.5194/acp-10-10541-2010, 2010.
- 614 Betts, A. K.: Diurnal variation of California coastal stratocumulus from two days of boundary layer soundings, *Tellus A*, 42(2),
615 302–304, doi:10.1034/j.1600-0870.1990.t01-1-00007.x, 1990.
- 616 Betts, A. K. and Boers, R.: A Cloudiness Transition in a Marine Boundary Layer, *J. Atmos. Sci.*, 47(12), 1480–1497,
617 doi:10.1175/1520-0469(1990)047<1480:ACTIAM>2.0.CO;2, 1990.
- 618 Bigg, E. K.: The supercooling of water, *Proc. Phys. Soc.*, B66, London, 688-694, 1953.
- 619 Bodas-Salcedo, A., Williams, K. D., Ringer, M. A., Beau, I., Cole, J. N. S., Dufresne, J. L., Koshiro, T., Stevens, B., Wang,
620 Z. and Yokohata, T.: Origins of the solar radiation biases over the Southern Ocean in CFMIP2 models, *J. Clim.*, 27(1),
621 41–56, doi:10.1175/JCLI-D-13-00169.1, 2014.

622 Bodas-Salcedo, A., Hill, P. G., Furtado, K., Williams, K. D., Field, P. R., Manners, J. C., Hyder, P. and Kato, S.: Large
623 contribution of supercooled liquid clouds to the solar radiation budget of the Southern Ocean, *J. Clim.*, 29(11), 4213–
624 4228, doi:10.1175/JCLI-D-15-0564.1, 2016.

625 Bony, S., Webb, M., Bretherton, C., Klein, S., Siebesma, P., Tselioudis, G. and Zhang, M.: CFMIP: Towards a better evaluation
626 and understanding of clouds and cloud feedbacks in CMIP5 models, *Clivar Exch.*, 56(2008), 2, 2011.

627 Bretherton, C. S., Wood, R., George, R. C., Leon, D., Allen, G. and Zheng, X.: Southeast Pacific stratocumulus clouds,
628 precipitation and boundary layer structure sampled along 20° S during VOCALS-REx, *Atmos. Chem. Phys.*, 10(21),
629 10639–10654, doi:10.5194/acp-10-10639-2010, 2010.

630 Brooks, M. E., Hogan, R. J. and Illingworth, A. J.: Parameterizing the Difference in Cloud Fraction Defined by Area and by
631 Volume as Observed with Radar and Lidar, *J. Atmos. Sci.*, 62(7), 2248–2260, doi:10.1175/JAS3467.1, 2005.

632 Bushell, A. C. and Martin, G. M.: The impact of vertical resolution upon GCM simulations of marine stratocumulus, *Clim.*
633 *Dyn.*, 15(4), 293–318, doi:10.1007/s003820050283, 1999.

634 Caldwell, P. and Bretherton, C. S.: [Response of a Subtropical Stratocumulus-Capped Mixed Layer to Climate and Aerosol](#)
635 [Changes, *J. Clim.*, 22\(1\), 20–38, doi:10.1175/2008JCLI1967.1, 2009.](#)

636 Caldwell, P. M., Zhang, Y. and Klein, S. A.: CMIP3 subtropical stratocumulus cloud feedback interpreted through a mixed-
637 layer model, *J. Clim.*, 26(5), 1607–1625, doi:10.1175/JCLI-D-12-00188.1, 2013.

638 Cesana, G. and Chepfer, H.: Evaluation of the cloud thermodynamic phase in a climate model using CALIPSO-GOCCP, *J.*
639 *Geophys. Res. Atmos.*, 118(14), 7922–7937, doi:10.1002/jgrd.50376, 2013.

640 Cesana, G., Waliser, D. E., Jiang, X. and Li, J. L. F.: Multimodel evaluation of cloud phase transition using satellite and
641 reanalysis data, *J. Geophys. Res. Atmos.*, 120(15), 7871–7892, doi:10.1002/2014JD022932, 2015.

642 Cesana, G., Chepfer, H., Winker, D., Getzewich, B., Cai, X., Jourdan, O., Mioche, G., Okamoto, H., Hagihara, Y., Noel, V.
643 and Reverdy, M.: Using in situ airborne measurements to evaluate three cloud phase products derived from CALIPSO,
644 *J. Geophys. Res. Atmos.*, 121(10), 5788–5808, doi:10.1002/2015JD024334, 2016.

645 Chin, M., Ginoux, P., Kinne, S., Torres, O., Holben, B. N., Duncan, B. N., Martin, R. V., Logan, J. a., Higurashi, A. and
646 Nakajima, T.: Tropospheric Aerosol Optical Thickness from the GOCART Model and Comparisons with Satellite and
647 Sun Photometer Measurements, *J. Atmos. Sci.*, 59(3), 461–483, doi:10.1175/1520-
648 0469(2002)059<0461:TAOTFT>2.0.CO;2, 2002.

649 Clarke, A. D., Owens, S. R. and Zhou, J.: An ultrafine sea-salt flux from breaking waves: Implications for cloud condensation
650 nuclei in the remote marine atmosphere, *J. Geophys. Res. Atmos.*, 111(6), 1–14, doi:10.1029/2005JD006565, 2006.

651 Collins, W. D.: Parameterization of Generalized Cloud Overlap for Radiative Calculations in General Circulation Models, *J.*
652 *Atmos. Sci.*, 58(21), 3224–3242, doi:10.1175/1520-0469(2001)058<3224:POGCOF>2.0.CO;2, 2001.

653 Cotton, W. R., Tripoli, G. J., Rauber, R. M. and Mulvihill, E. a.: Numerical Simulation of the Effects of Varying Ice Crystal
654 Nucleation Rates and Aggregation Processes on Orographic Snowfall, *J. Clim. Appl. Meteorol.*, 25(11), 1658–1680,
655 doi:10.1175/1520-0450(1986)025<1658:NSOTEO>2.0.CO;2, 1986.

656 Covert, D. S., Kapustin, V. N., Bates, T. S. and Quinn, P. K.: Physical properties of marine boundary layer aerosol particles
657 of the mid-Pacific in relation to sources and meteorological transport, *J. Geophys. Res. Atmos.*, 101(D3), 6919–6930,
658 doi:10.1029/95JD03068, 1996.

659 Deardorff, J. W.: Cloud Top Entrainment Instability, *J. Atmos. Sci.*, 37(1), 131–147, doi:10.1175/1520-
660 0469(1980)037<0131:CTEI>2.0.CO;2, 1980.

661 Duynkerke, P. G. and Teixeira, J.: Comparison of the ECMWF Reanalysis with FIRE I Observations: Diurnal Variation of
662 Marine Stratocumulus, *J. Clim.*, 14(7), 1466–1478, doi:10.1175/1520-0442(2001)014<1466:COTERW>2.0.CO;2, 2001.

663 ECMWF: Clouds and large-scale precipitation, IFS Documentation, European Centre for Medium-Range Weather Forecasts,
664 CY25r1, Part IV, Chapter 6, 2002.

665 ECMWF: Clouds and large-scale precipitation, IFS Documentation, European Centre for Medium-Range Weather Forecasts,
666 CY43r3, Part IV, Chapter 7, 2017.

667 Eyring, V., Bony, S., Meehl, G. A., Senior, C., Stevens, B., Stouffer, R. J. and Taylor, K. E.: Overview of the Coupled Model
668 Intercomparison Project Phase 6 (CMIP6) experimental design and organisation, *Geosci. Model Dev. Discuss.*, 8(12),
669 10539–10583, doi:10.5194/gmdd-8-10539-2015, 2015.

670 Forbes, R. M. and Ahlgrimm, M.: On the Representation of High-Latitude Boundary Layer Mixed-Phase Cloud in the ECMWF
671 Global Model, *Mon. Weather Rev.*, 142(9), 3425–3445, doi:10.1175/MWR-D-13-00325.1, 2014.

672 Forbes, R. M., Geer, A., Lonitz, K., and Ahlgrimm, M.: Reducing systematic errors in cold-air outbreaks, *ECMWF Newsletter*,
673 No. 146, European Centre for Medium-Range Weather Forecasts, 17–22, <https://doi.org/10.21957/s41h7q71>, 2016.

674 Frey, W. R. and Kay, J. E.: The influence of extratropical cloud phase and amount feedbacks on climate sensitivity, *Clim.*
675 *Dyn.*, 50(7–8), 3097–3116, doi:10.1007/s00382-017-3796-5, 2018.

676 Geleyn, J.-F., and Hollingsworth, A.: An economical analytical method for the computation of the interaction between
677 scattering and line absorption of radiation, *Beitr. Phys. Atmos.*, 52, 1-16, 1979.

678 Guo, Z., Wang, M., Qian, Y., Larson, V. E., Ghan, S., Ovchinnikov, M., Bogenschutz, P. A., Zhao, C., Lin, G. and Zhou, T.:
679 A sensitivity analysis of cloud properties to CLUBB parameters in the single-column Community Atmosphere Model
680 (SCAM5), *J. Adv. Model. Earth Syst.*, 6(3), 829–858, doi:10.1002/2014MS000315, 2015.

681 Hahn, C. J., and Warren, S. G.: Extended edited synoptic cloud reports from ships and land stations over the globe, 1952–1996
682 (2009 update). NDP-026C, Carbon Dioxide Information Analysis Center, Oak Ridge National Laboratory, Oak Ridge,
683 TN, 2009.

684 Heymsfield, A. J.: Precipitation Development in Stratiform Ice Clouds: A Microphysical and Dynamical Study, *J. Atmos. Sci.*,
685 34(2), 367–381, doi:10.1175/1520-0469(1977)034<0367:PDISIC>2.0.CO;2, 1977.

686 Heymsfield, A. J. and Donner, L. J.: A Scheme for Parameterizing Ice-Cloud Water Content in General Circulation Models,
687 *J. Atmos. Sci.*, 47(15), 1865–1877, doi:10.1175/1520-0469(1990)047<1865:ASFPIC>2.0.CO;2, 1990.

688 Heymsfield, A. J. and Iaquinta, J.: Cirrus Crystal Terminal Velocities, *J. Atmos. Sci.*, 57(7), 916–938, doi:10.1175/1520-
689 0469(2000)057<0916:CCTV>2.0.CO;2, 2000.

690 Hoose, C., Kristjánsson, J. E., Iversen, T., Kirkevåg, A., Seland, Ø. and Gettelman, A.: Constraining cloud droplet number
691 concentration in GCMs suppresses the aerosol indirect effect, *Geophys. Res. Lett.*, 36(12), L12807,
692 doi:10.1029/2009GL038568, 2009.

693 Hu, Y., Rodier, S., Xu, K. M., Sun, W., Huang, J., Lin, B., Zhai, P. and Josset, D.: Occurrence, liquid water content, and
694 fraction of supercooled water clouds from combined CALIOP/IIR/MODIS measurements, *J. Geophys. Res. Atmos.*,
695 115(19), 1–13, doi:10.1029/2009JD012384, 2010.

696 Jakob, C.: The representation of cloud cover in Atmospheric General Circulation Models, A thesis submitted to the Fakultät
697 für Physik der Ludwig-Maximilians-Universität, European Centre for Medium-Range Weather Forecasts, 2000.

698 Jiang, J. H., Su, H., Zhai, C., Perun, V. S., Del Genio, A., Nazarenko, L. S., Donner, L. J., Horowitz, L., Seman, C., Cole, J.,
699 Gettelman, A., Ringer, M. a., Rotstayn, L., Jeffrey, S., Wu, T., Brient, F., Dufresne, J. L., Kawai, H., Kosshiro, T.,
700 Watanabe, M., Lécuyer, T. S., Volodin, E. M., Iversen, T., Drange, H., Mesquita, M. D. S., Read, W. G., Waters, J. W.,
701 Tian, B., Teixeira, J. and Stephens, G. L.: Evaluation of cloud and water vapor simulations in CMIP5 climate models
702 Using NASA “A-Train” satellite observations, *J. Geophys. Res. Atmos.*, 117(14), doi:10.1029/2011JD017237, 2012.

703 Jones, A., Roberts, D. L., Woodage, M. J. and Johnson, C. E.: Indirect sulphate aerosol forcing in a climate model with an
704 interactive sulphur cycle, *J. Geophys. Res. Atmos.*, 106(D17), 20293–20310, doi:10.1029/2000JD000089, 2001.

705 Kärcher, B. and Lohmann, U.: A Parameterization of cirrus cloud formation: Homogeneous freezing including effects of
706 aerosol size, *J. Geophys. Res. Atmos.*, 107(D23), AAC 9-1-AAC 9-10, doi:10.1029/2001JD001429, 2002.

707 Kärcher, B., and Lohmann, U.: A parameterization of cirrus cloud formation: Heterogeneous freezing, *J. Geophys. Res.*, 108,
708 D14, 4402, <https://doi.org/10.1029/2002JD003220>, 2003.

709 Kärcher, B., Hendricks, J. and Lohmann, U.: Physically based parameterization of cirrus cloud formation for use in global
710 atmospheric models, *J. Geophys. Res.*, 111(D1), 1–11, doi:10.1029/2005JD006219, 2006.

711 Kawai, H.: Improvement of a Cloud Ice Fall Scheme in GCM, CAS/JSC WGNE Research Activities in Atmospheric and
712 Oceanic Modelling/WMO, 35, 4.11-4.12, 2005.

713 Kawai, H.: Improvement of a Stratocumulus Scheme for Mid-latitude Marine Low Clouds, CAS/JSC WGNE Research
714 Activities in Atmospheric and Oceanic Modelling/WMO, 43, 4.03-4.04, 2013.

715 Kawai, H. and Inoue, T.: A simple parameterization scheme for subtropical marine stratocumulus, *Sci. Online Lett. Atmos.*, 2,
716 doi:10.2151/sola.2006-005, 2006.

717 Kawai, H., Yabu, S., Hagihara, Y., Kosshiro, T. and Okamoto, H.: Characteristics of the cloud top heights of marine boundary
718 layer clouds and the frequency of marine fog over mid-latitudes, *J. Meteorol. Soc. Japan*, 93(6), doi:10.2151/jmsj.2015-
719 045, 2015.

720 Kawai, H., Kosshiro, T., Webb, M., Yukimoto, S., and Tanaka, T.: Cloud feedbacks in MRI-CGCM3, CAS/JSC WGNE
721 Research Activities in Atmospheric and Oceanic Modelling/WMO, 45, 7.11-7.12, 2015.

722 Kawai, H., Kosshiro, T. and Webb, M. J.: Interpretation of factors controlling low cloud cover and low cloud feedback using a
723 unified predictive index, *J. Clim.*, 30(22), doi:10.1175/JCLI-D-16-0825.1, 2017.

724 Kawai, H., Koshiro, T., Endo, H. and Arakawa, O.: Changes in marine fog over the North Pacific under different climates in
725 CMIP5 multimodel simulations, *J. Geophys. Res. Atmos.*, 123(19), 10911–10924, doi:10.1029/2018JD028899, 2018.

726 Kay, J. E., Wall, C., Yettella, V., Medeiros, B., Hannay, C., Caldwell, P. and Bitz, C.: Global climate impacts of fixing the
727 Southern Ocean shortwave radiation bias in the Community Earth System Model (CESM), *J. Clim.*, 0–53,
728 doi:10.1017/CBO9781107415324.004, 2016.

729 Klein, S. A. and Hartmann, D. L.: The seasonal cycle of low stratiform clouds, *J. Clim.*, 6(8), 1587–1606, doi:10.1175/1520-
730 0442(1993)006<1587:TSCOLS>2.0.CO;2, 1993.

731 Koshiro, T., Shiotani, M., Kawai, H. and Yukimoto, S.: Evaluation of Relationships between Subtropical Marine Low
732 Stratiform Cloudiness and Estimated Inversion Strength in CMIP5 Models Using the Satellite Simulator Package COSP,
733 SOLA, 14(0), 25–32, doi:10.2151/sola.2018-005, 2018.

734 Kuo, H.-C. and Schubert, W. H.: Stability of cloud-topped boundary layers, *Q. J. R. Meteorol. Soc.*, 114(482), 887–916,
735 doi:10.1002/qj.49711448204, 1988.

736 [Larson, K., Hartmann, D. L. and Klein, S. a.: The Role of Clouds, Water Vapor, Circulation, and Boundary Layer Structure in
737 the Sensitivity of the Tropical Climate, *J. Clim.*, 12\(8\), 2359–2374, doi:10.1175/1520-
738 0442\(1999\)012<2359:TROCWV>2.0.CO;2, 1999.](#)

739 [Lauer, A. and Hamilton, K.: Simulating Clouds with Global Climate Models: A Comparison of CMIP5 Results with CMIP3
740 and Satellite Data, *J. Clim.*, 26\(11\), 3823–3845, doi:10.1175/JCLI-D-12-00451.1, 2013.](#)

741 [Lauer, A., Hamilton, K., Wang, Y., Phillips, V. T. J. and Bennartz, R.: The Impact of Global Warming on Marine Boundary
742 Layer Clouds over the Eastern Pacific—A Regional Model Study, *J. Clim.*, 23\(21\), 5844–5863,
743 doi:10.1175/2010JCLI3666.1, 2010.](#)

744 Levkov, L., Rockel, B., Kapitza, H., and Raschke, E.: 3D mesoscale numerical studies of cirrus and stratus clouds by their
745 time and space evolution, *Beitr. Phys. Atmos.*, 65, 35–58, 1992.

746 Li, J. L. F., Waliser, D. E., Stephens, G., Lee, S., L’Ecuyer, T., Kato, S., Loeb, N. and Ma, H. Y.: Characterizing and
747 understanding radiation budget biases in CMIP3/CMIP5 GCMs, contemporary GCM, and reanalysis, *J. Geophys. Res.*
748 *Atmos.*, 118(15), 8166–8184, doi:10.1002/jgrd.50378, 2013.

749 Liu, X., Easter, R. C., Ghan, S. J., Zaveri, R., Rasch, P., Shi, X., Lamarque, J. F., Gettelman, A., Morrison, H., Vitt, F., Conley,
750 A., Park, S., Neale, R., Hannay, C., Ekman, A. M. L., Hess, P., Mahowald, N., Collins, W., Iacono, M. J., Bretherton, C.
751 S., Flanner, M. G. and Mitchell, D.: Toward a minimal representation of aerosols in climate models: Description and
752 evaluation in the Community Atmosphere Model CAM5, *Geosci. Model Dev.*, 5(3), 709–739, doi:10.5194/gmd-5-709-
753 2012, 2012.

754 Lock, A. P.: Factors influencing cloud area at the capping inversion for shallow cumulus clouds, *Q. J. R. Meteorol. Soc.*,
755 135(641), 941–952, doi:10.1002/qj.424, 2009.

756 Loeb, N. G., Wielicki, B. A., Doelling, D. R., Smith, G. L., Keyes, D. F., Kato, S., Manalo-Smith, N. and Wong, T.: Toward
757 Optimal Closure of the Earth's Top-of-Atmosphere Radiation Budget, *J. Clim.*, 22(3), 748–766,
758 doi:10.1175/2008JCLI2637.1, 2009.

759 Lohmann, U.: Possible Aerosol Effects on Ice Clouds via Contact Nucleation, *J. Atmos. Sci.*, 59(3), 647–656,
760 doi:10.1175/1520-0469(2001)059<0647:PAEOIC>2.0.CO;2, 2002.

761 Lohmann, U. and Diehl, K.: Sensitivity Studies of the Importance of Dust Ice Nuclei for the Indirect Aerosol Effect on
762 Stratiform Mixed-Phase Clouds, *J. Atmos. Sci.*, 63(3), 968–982, doi:10.1175/JAS3662.1, 2006.

763 Lohmann, U., Stier, P., Hoose, C., Ferrachat, S., Kloster, S., Roeckner, E. and Zhang, J.: Cloud microphysics and aerosol
764 indirect effects in the global climate model ECHAM5-HAM, *Atmos. Chem. Phys.*, 7(13), 3425–3446, doi:10.5194/acp-
765 7-3425-2007, 2007.

766 MacVean, M. K.: A Numerical Investigation of the Criterion for Cloud-Top Entrainment Instability, *J. Atmos. Sci.*, 50(15),
767 2481–2495, doi:10.1175/1520-0469(1993)050<2481:ANIOTC>2.0.CO;2, 1993.

768 MacVean, M. K. and Mason, P. J.: Cloud-Top Entrainment Instability through Small-Scale Mixing and Its Parameterization
769 in Numerical Models, *J. Atmos. Sci.*, 47(8), 1012–1030, doi:10.1175/1520-0469(1990)047<1012:CTEITS>2.0.CO;2,
770 1990.

771 Manton, M. J., and Cotton, W. R.: Formulation of approximate equations for modeling moist deep convection on the mesoscale,
772 Atmospheric Science Paper, No. 266, Colorado State University, 1977.

773 Mauritsen, T., Stevens, B., Roeckner, E., Crueger, T., Esch, M., Giorgetta, M., Haak, H., Jungclaus, J., Klocke, D., Matei, D.,
774 Mikolajewicz, U., Notz, D., Pincus, R., Schmidt, H. and Tomassini, L.: Tuning the climate of a global model, , 4, 1–18,
775 doi:10.1029/2012MS000154, 2012.

776 McCoy, D. T., Hartmann, D. L., Zelinka, M. D., Ceppi, P. and Grosvenor, D. P.: Mixed-phase cloud physics and Southern
777 Ocean cloud feedback in climate models, *J. Geophys. Res. Atmos.*, 120(18), 9539–9554, doi:10.1002/2015JD023603,
778 2015.

779 McFarquhar, G. M. and Heymsfield, A. J.: Parameterization of Tropical Cirrus Ice Crystal Size Distributions and Implications
780 for Radiative Transfer: Results from CEPEX, *J. Atmos. Sci.*, 54(17), 2187–2200, doi:10.1175/1520-
781 0469(1997)054<2187:POTCIC>2.0.CO;2, 1997.

782 [Medeiros, B., Stevens, B., Held, I. M., Zhao, M., Williamson, D. L., Olson, J. G. and Bretherton, C. S.: Aquaplanets, Climate](#)
783 [Sensitivity, and Low Clouds, *J. Clim.*, 21\(19\), 4974–4991, doi:10.1175/2008JCLI1995.1, 2008.](#)

784 Meyers, M. P., DeMott, P. J. and Cotton, W. R.: New Primary Ice-Nucleation Parameterizations in an Explicit Cloud Model,
785 *J. Appl. Meteorol.*, 31(7), 708–721, doi:10.1175/1520-0450(1992)031<0708:NPINPI>2.0.CO;2, 1992.

786 [Miller, R. L.: Tropical Thermostats and Low Cloud Cover, *J. Clim.*, 10\(3\), 409–440, doi:10.1175/1520-](#)
787 [0442\(1997\)010<0409:TTALCC>2.0.CO;2, 1997.](#)

788 [Morrison, H. and Gettelman, A.: A New Two-Moment Bulk Stratiform Cloud Microphysics Scheme in the Community](#)
789 [Atmosphere Model, Version 3 \(CAM3\). Part I: Description and Numerical Tests, J. Clim., 21\(15\), 3642–3659,](#)
790 [doi:10.1175/2008JCLI2105.1, 2008.](#)

791 Murakami, M.: Numerical Modeling of Dynamical and Microphysical Evolution of an Isolated Convective Cloud - The 19
792 July 1981 CCOPE cloud, J. Meteor. Soc. Japan, 68(April), 107–128, doi:10.2151/jmsj1965.68.2_107, 1990.

793 Nagasawa, R.: The Problem of Cloud Overlap in the Radiation Process of JMA's Global NWP Model, CAS/JSC WGNE
794 Research Activities in Atmospheric and Oceanic Modelling/WMO, 42, 0415-0416, 2012.

795 Nam, C., Bony, S., Dufresne, J. L. and Chepfer, H.: The too few, too bright tropical low-cloud problem in CMIP5 models,
796 Geophys. Res. Lett., 39(21), 1–7, doi:10.1029/2012GL053421, 2012.

797 Neubauer, D., Lohmann, U., Hoese, C. and Frontoso, M. G.: Impact of the representation of marine stratocumulus clouds on
798 the anthropogenic aerosol effect, Atmos. Chem. Phys., 14(21), 11997–12022, doi:10.5194/acp-14-11997-2014, 2014.

799 Nuijens, L., Medeiros, B., Sandu, I. and Ahlgrimm, M.: The behavior of trade-wind cloudiness in observations and models:
800 The major cloud components and their variability, J. Adv. Model. Earth Syst., 7(2), 600–616,
801 doi:10.1002/2014MS000390, 2015.

802 Pincus, R., Platnick, S., Ackerman, S. A., Hemler, R. S. and Patrick Hofmann, R. J.: Reconciling simulated and observed
803 views of clouds: MODIS, ISCCP, and the limits of instrument simulators, J. Clim., 25(13), 4699–4720,
804 doi:10.1175/JCLI-D-11-00267.1, 2012.

805 [Qu, X., Hall, A., Klein, S. A. and Caldwell, P. M.: On the spread of changes in marine low cloud cover in climate model](#)
806 [simulations of the 21st century, Clim. Dyn., 42\(9–10\), 2603–2626, doi:10.1007/s00382-013-1945-z, 2014.](#)

807 Rahn, D. A. and Garreaud, R.: Marine boundary layer over the subtropical southeast Pacific during VOCALS-REx – Part 1:
808 Mean structure and diurnal cycle, Atmos. Chem. Phys., 10(10), 4491–4506, doi:10.5194/acp-10-4491-2010, 2010.

809 Randall, D. A.: Conditional Instability of the First Kind Upside-Down, J. Atmos. Sci., 37(1), 125–130, doi:10.1175/1520-
810 0469(1980)037<0125:CIOTFK>2.0.CO;2, 1980.

811 Rossow, W. B. and Schiffer, R. A.: Advances in Understanding Clouds from ISCCP, Bull. Am. Meteorol. Soc., 80(11), 2261–
812 2287, doi:10.1175/1520-0477(1999)080<2261:AIUCFI>2.0.CO;2, 1999.

813 Rotstayn, L. D.: A physically based scheme for the treatment of stratiform clouds and precipitation in large-scale models. I:
814 Description and evaluation of the microphysical processes, Q. J. R. Meteorol. Soc., 123(541), 1227–1282,
815 doi:10.1002/qj.49712354106, 1997.

816 Rotstayn, L. D.: On the “tuning” of autoconversion parameterizations in climate models, J. Geophys. Res. Atmos., 105(D12),
817 15495–15507, doi:10.1029/2000JD900129, 2000.

818 Rutledge, S. a. and Hobbs, P.: The Mesoscale and Microscale Structure and Organization of Clouds and Precipitation in
819 Midlatitude Cyclones. VIII: A Model for the “Seeder-Feeder” Process in Warm-Frontal Rainbands, J. Atmos. Sci., 40(5),
820 1185–1206, doi:10.1175/1520-0469(1983)040<1185:TMAMSA>2.0.CO;2, 1983.

821 Seinfeld, J. H., and Pandis, S. N.: *Atmospheric Chemistry and Physics: From Air Pollution to Climate Change* 2nd ed, John
822 Wiley & Sons, New York, USA, 1203, 2006.

823 Siebesma, A. P., Jakob, C., Lenderink, G., Neggers, R. A. J., Teixeira, J., van Meijgaard, E., Calvo, J., Chlond, A., Grenier,
824 H., Jones, C., Köhler, M., Kitagawa, H., Marquet, P., Lock, A. P., Müller, F., Olmeda, D. C. and Severijns, C.: Cloud
825 representation in general-circulation models over the northern Pacific Ocean: A EUROCS intercomparison study, *Q. J.*
826 *R. Meteorol. Soc.*, 130(604), 3245–3267, doi:10.1256/qj.03.146, 2004.

827 Slingo, J. M.: A cloud parametrization scheme derived from GATE data for use with a numerical model, *Q. J. R. Meteorol.*
828 *Soc.*, 106(450), 747–770, doi:10.1002/qj.49710645008, 1980.

829 Slingo, J. M.: The Development and Verification of A Cloud Prediction Scheme For the Ecmwf Model, *Q. J. R. Meteorol.*
830 *Soc.*, 113(477), 899–927, doi:10.1002/qj.49711347710, 1987.

831 Smith, R. N. B.: A scheme for predicting layer clouds and their water content in a general circulation model, *Q. J. R. Meteorol.*
832 *Soc.*, 116(492), 435–460, doi:10.1002/qj.49711649210, 1990.

833 Soden, B. J. and Held, I. M.: An Assessment of Climate Feedbacks in Coupled Ocean – Atmosphere Models, *J. Clim.*, 19(2003),
834 3354–3360, doi:10.1175/JCLI9028.1, 2006.

835 Soden, B. J., Held, I. M., Colman, R. C., Shell, K. M., Kiehl, J. T. and Shields, C. A.: Quantifying climate feedbacks using
836 radiative kernels, *J. Clim.*, 21(14), 3504–3520, doi:10.1175/2007JCLI2110.1, 2008.

837 Su, H., Jiang, J. H., Zhai, C., Perun, V. S., Shen, J. T., Del Genio, A., Nazarenko, L. S., Donner, L. J., Horowitz, L., Seman,
838 C., Morcrette, C., Petch, J., Ringer, M., Cole, J., Von Salzen, K., Mesquita, M. D. S., Iversen, T., Kristjansson, J. E.,
839 Gettelman, A., Rotstayn, L., Jeffrey, S., Dufresne, J. L., Watanabe, M., Kawai, H., Koshiro, T., Wu, T., Volodin, E. M.,
840 L’Ecuyer, T., Teixeira, J. and Stephens, G. L.: Diagnosis of regime-dependent cloud simulation errors in CMIP5 models
841 using “a-Train” satellite observations and reanalysis data, *J. Geophys. Res. Atmos.*, 118(7), 2762–2780,
842 doi:10.1029/2012JD018575, 2013.

843 Suzuki, K., Stephens, G., Bodas-Salcedo, A., Wang, M., Golaz, J.-C., Yokohata, T. and Koshiro, T.: Evaluation of the Warm
844 Rain Formation Process in Global Models with Satellite Observations, *J. Atmos. Sci.*, 72(10), 3996–4014,
845 doi:10.1175/JAS-D-14-0265.1, 2015.

846 Takemura, T., Nozawa, T., Emori, S., Nakajima, T. Y. and Nakajima, T.: Simulation of climate response to aerosol direct and
847 indirect effects with aerosol transport-radiation model, *J. Geophys. Res. D Atmos.*, 110(2), 1–16,
848 doi:10.1029/2004JD005029, 2005.

849 Tan, I. and Storelmo, T.: Sensitivity Study on the Influence of Cloud Microphysical Parameters on Mixed-Phase Cloud
850 Thermodynamic Phase Partitioning in CAM5, *J. Atmos. Sci.*, 73(2), 709–728, doi:10.1175/JAS-D-15-0152.1, 2016.

851 Tan, I., Storelmo, T. and Zelinka, M. D.: Observational constraints on mixed-phase clouds imply higher climate sensitivity,
852 *Science* (80-.), 352(6282), 224–227, doi:10.1126/science.aad5300, 2016.

853 Tanaka, T. Y., Orito, K., Sekiyama, T. T., Shibata, K., Chiba, M. and Tanaka, H.: MASINGAR, a global tropospheric aerosol
854 chemical transport model coupled with MRI/JMA98 GCM: Model description, *Pap. Meteorol. Geophys.*, 53(4), 119–
855 138, doi:10.2467/mripapers.53.119, 2003.

856 Taylor, K. E.: Summarizing multiple aspects of model performance in a single diagram, *J. Geophys. Res. Atmos.*, 106(D7),
857 7183–7192, doi:10.1029/2000JD900719, 2001.

858 Taylor, K. E., Stouffer, R. J. and Meehl, G. A.: An Overview of CMIP5 and the Experiment Design, *Bull. Am. Meteorol. Soc.*,
859 93(4), 485–498, doi:10.1175/BAMS-D-11-00094.1, 2012.

860 Teixeira, J.: The impact of increased boundary layer vertical resolution on the ECMWF forecast system, ECMWF technical
861 memorandum, European Centre for Medium-Range Weather Forecasts, 268, 1-55, 1999.

862 Tiedtke, M.: Representation of Clouds in Large-Scale Models, *Mon. Wea. Rev.*, 121, 3040–3061, 1993.

863 Trenberth, K. E. and Fasullo, J. T.: Simulation of present-day and twenty-first-century energy budgets of the southern oceans,
864 *J. Clim.*, 23(2), 440–454, doi:10.1175/2009JCLI3152.1, 2010.

865 Tsushima, Y., Emori, S., Ogura, T., Kimoto, M., Webb, M. J., Williams, K. D., Ringer, M. A., Soden, B. J., Li, B. and
866 Andronova, N.: Importance of the mixed-phase cloud distribution in the control climate for assessing the response of
867 clouds to carbon dioxide increase: a multi-model study, *Clim. Dyn.*, 27(2–3), 113–126, doi:10.1007/s00382-006-0127-7,
868 2006.

869 Tsushima, Y., Ringer, M. A., Webb, M. J. and Williams, K. D.: Quantitative evaluation of the seasonal variations in climate
870 model cloud regimes, *Clim. Dyn.*, 41(9–10), 2679–2696, doi:10.1007/s00382-012-1609-4, 2013.

871 Tsushima, Y., Ringer, M. A., Koshiro, T., Kawai, H., Roehrig, R., Cole, J., Watanabe, M., Yokohata, T., Bodas-Salcedo, A.,
872 Williams, K. D. and Webb, M. J.: Robustness, uncertainties, and emergent constraints in the radiative responses of
873 stratocumulus cloud regimes to future warming, *Clim. Dyn.*, 46(9–10), doi:10.1007/s00382-015-2750-7, 2016.

874 Uppala, S. M., KÅllberg, P. W., Simmons, A. J., Andrae, U., Bechtold, V. D. C., Fiorino, M., Gibson, J. K., Haseler, J.,
875 Hernandez, A., Kelly, G. A., Li, X., Onogi, K., Saarinen, S., Sokka, N., Allan, R. P., Andersson, E., Arpe, K., Balmaseda,
876 M. A., Beljaars, A. C. M., Berg, L. Van De, Bidlot, J., Bormann, N., Caires, S., Chevallier, F., Dethof, A., Dragosavac,
877 M., Fisher, M., Fuentes, M., Hagemann, S., Hólm, E., Hoskins, B. J., Isaksen, I., Janssen, P. A. E. M., Jenne, R., McNally,
878 A. P., Mahfouf, J.-F., Morcrette, J.-J., Rayner, N. A., Saunders, R. W., Simon, P., Sterl, A., Trenberth, K. E., Untch, A.,
879 Vasiljevic, D., Viterbo, P. and Woollen, J.: The ERA-40 re-analysis, *Q. J. R. Meteorol. Soc.*, 131(612), 2961–3012,
880 doi:10.1256/qj.04.176, 2005.

881 Wang, Y., Xu, H. and Xie, S.-P.: Regional Model Simulations of Marine Boundary Layer Clouds over the Southeast Pacific
882 off South America. Part II: Sensitivity Experiments*, *Mon. Weather Rev.*, 132(11), 2650–2668,
883 doi:10.1175/MWR2812.1, 2004.

884 Webb, M. J., [Lambert, F. H. and Gregory, J. M.: Origins of differences in climate sensitivity, forcing and feedback in climate](#)
885 [models, *Clim. Dyn.*, 40\(3–4\), 677–707, doi:10.1007/s00382-012-1336-x, 2013](#) ~~Andrews, T., Bodas-salcedo, A., Bony, S.,~~
886 ~~Bretherton, C. S., Chadwick, R., Chepfer, H., Douville, H., Good, P., Kay, J. E., Klein, S. A., Marchand, R., Medeiros,~~

887 [B., Siebesma, A. P., Skinner, C. B. and Stevens, B.: The Cloud Feedback Model Intercomparison Project \(CFMIP \)](#)
888 [contribution to CMIP6, \(7\), 359–384, doi:10.5194/gmd-10-359-2017, 2017.](#)

889 [Webb, M. J., Andrews, T., Bodas-salcedo, A., Bony, S., Bretherton, C. S., Chadwick, R., Chepfer, H., Douville, H., Good, P.,](#)
890 [Kay, J. E., Klein, S. A., Marchand, R., Medeiros, B., Siebesma, A. P., Skinner, C. B. and Stevens, B.: The Cloud Feedback](#)
891 [Model Intercomparison Project \(CFMIP \) contribution to CMIP6, \(7\), 359–384, doi:10.5194/gmd-10-359-2017, 2017.](#)

892 [Williams, K. D., Ringer, M. A., Senior, C. A., Webb, M. J., McAvaney, B. J., Andronova, N., Bony, S., Dufresne, J. L., Emori,](#)
893 [S., Gudgel, R., Knutson, T., Li, B., Lo, K., Musat, I., Wegner, J., Slingo, A. and Mitchell, J. F. B.: Evaluation of a](#)
894 [component of the cloud response to climate change in an intercomparison of climate models, *Clim. Dyn.*, 26\(2–3\), 145–](#)
895 [165, doi:10.1007/s00382-005-0067-7, 2006.](#)

896 Wilson, D. R., Smith, R. N. B., Gregory, D., Wilson, C. A., Bushell, A. C., and Cusack, S.: The large-scale cloud scheme and
897 saturated specific humidity, Unified Model documentation paper, 29, Met Office, Exeter, UK, 2007.

898 Wilson, D. R., Bushell, A. C., Kerr-Munslow, A. M., Price, J. D., Morcrette, C. J. and Bodas-Salcedo, A.: PC2: A prognostic
899 cloud fraction and condensation scheme. II: Climate model simulations, *Q. J. R. Meteorol. Soc.*, 134(637), 2109–2125,
900 doi:10.1002/qj.332, 2008.

901 Winker, D. M., Vaughan, M. A., Omar, A., Hu, Y., Powell, K. A., Liu, Z., Hunt, W. H. and Young, S. A.: Overview of the
902 CALIPSO Mission and CALIOP Data Processing Algorithms, *J. Atmos. Ocean. Technol.*, 26(11), 2310–2323,
903 doi:10.1175/2009JTECHA1281.1, 2009.

904 Wood, R.: Stratocumulus Clouds, *Mon. Weather Rev.*, 140(8), 2373–2423, doi:10.1175/MWR-D-11-00121.1, 2012.

905 Wood, R. and Bretherton, C. S.: On the relationship between stratiform low cloud cover and lower-tropospheric stability, *J.*
906 *Clim.*, 19(24), 6425–6432, doi:10.1175/JCLI3988.1, 2006.

907 Yamaguchi, T. and Randall, D. A.: Large-Eddy Simulation of Evaporatively Driven Entrainment in Cloud-Topped Mixed
908 Layers, *J. Atmos. Sci.*, 65(5), 1481–1504, doi:10.1175/2007JAS2438.1, 2008.

909 Yukimoto, S., Yoshimura, H., Hosaka, M., Sakami, T., Tsujino, H., Hirabara, M., Tanaka, T. Y., Deushi, M., Obata, A.,
910 Nakano, H., Adachi, Y., Shindo, E., Yabu, S., Ose, T., and Kitoh, A.: Meteorological Research Institute Earth System
911 Model Version 1 (MRI-ESM1)—Model Description—, *Tech. Rep. of MRI*, 64, 83 pp, available at: [http://www.mri-](http://www.mri-jma.go.jp/Publish/Technical/index_en.html)
912 [jma.go.jp/Publish/Technical/index_en.html](http://www.mri-jma.go.jp/Publish/Technical/index_en.html), 2011.

913 Yukimoto, S., Adachi, Y., Hosaka, M., Sakami, T., Yoshimura, H., Hirabara, M., Tanaka, T. Y., Shindo, E., Tsujino, H.,
914 Deushi, M., Mizuta, R., Yabu, S., Obata, A., Nakano, H., Koshiro, T., Ose, T., and Kitoh, A.: A new global climate model
915 of the Meteorological Research Institute: MRI-CGCM3 --Model Description and Basic Performance--, *J. Meteorol. Soc.*
916 *Japan*, 90A(0), 23–64, <https://doi.org/10.2151/jmsj.2012-A02>, 2012.

917 [Yukimoto, S., Kawai, H., Koshiro, T., Oshima, N., Yoshida, K., Urakawa, S., Tsujino, H., Deushi, M., Tanaka, T., Hosaka,](#)
918 [M., Yabu, S., Yoshimura, H., Shindo, E., Mizuta, R., Obata, A., Adachi, Y. and Ishii, M.: The Meteorological Research](#)
919 [Institute Earth System Model version 2.0, MRI-ESM2.0: Description and basic evaluation of the physical component, *J.*](#)
920 [Meteor. Soc. Japan](#), 97, in press, <https://doi.org/10.2151/jmsj.2019-051>, 2019.

921 Zhang, Y., Xie, S., Covey, C., Lucas, D. D., Gleckler, P., Klein, S. A., Tannahill, J., Doutriaux, C. and Klein, R.: Regional
922 assessment of the parameter-dependent performance of CAM4 in simulating tropical clouds, *Geophys. Res. Lett.*, 39(14),
923 1–7, doi:10.1029/2012GL052184, 2012.

924 Zurovac-Jevtić, D. and Zhang, G. J.: Development and Test of a Cirrus Parameterization Scheme Using NCAR CCM3, *J.*
925 *Atmos. Sci.*, 60(11), 1325–1344, doi:10.1175/1520-0469(2003)060<1325:DATOAC>2.0.CO;2, 2003.

926

927

928

Experiments	Section
Control (time step = 3600 s, 1800 s [default], 900 s, and 300 s)	
with an old version of stratocumulus scheme	3.1
with an old treatment of the WBF effect	3.2
shallow convection can be active even under stratocumulus conditions	3.3
shallow convection can be active even under stratocumulus conditions using L48	3.4
with an old version of cloud overlap scheme	3.5
radiation calculation for every two latitudinal grids	3.6
1-hourly longwave radiation calculation	3.6
using original (not doubled) number concentration of sea salt CCN	3.8
with an old version of ice fall scheme (time step = 3600 s, 1800 s, 900 s, and 300 s)	3.9

929

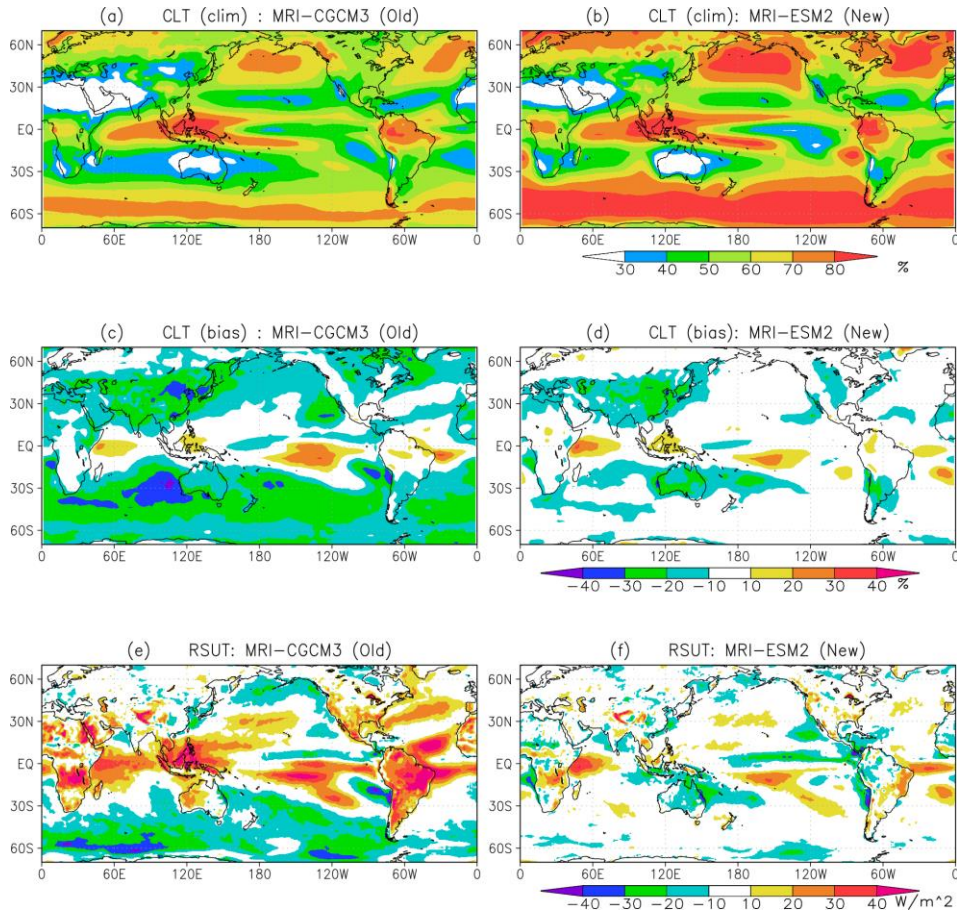
930 **Table 1: List of sensitivity experiments performed in the present study using MRI-ESM2 to identify the effect of each modification.**
931 **The second column shows the section in which each modification is discussed.**

932

933

934

935



937

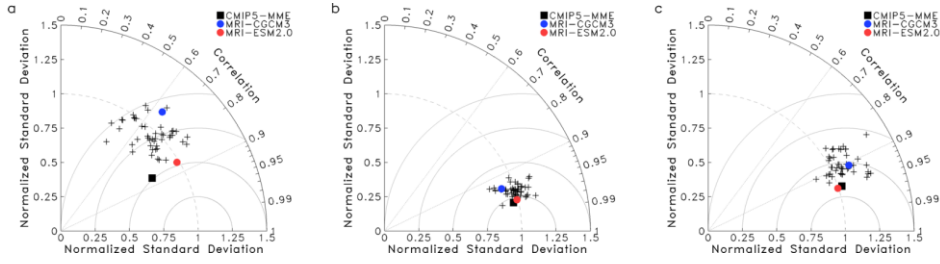
938 **Figure 2:** (a, b) Climatologies of total cloud cover (%), (c, d) biases of total cloud cover (%) with respect to ISCCP observations, and
 939 (e, f) biases of upward shortwave radiative flux ($W m^{-2}$) at the top of the atmosphere with respect to CERES-EBAF simulated by (a,
 940 c, e) MRI-CGCM3 and (b, d, f) MRI-ESM2. The climatologies cover the period 1986–2005 for model simulations and ISCCP
 941 observational data, and 2001–2010 for CERES-EBAF data.

942

943

944

945



946

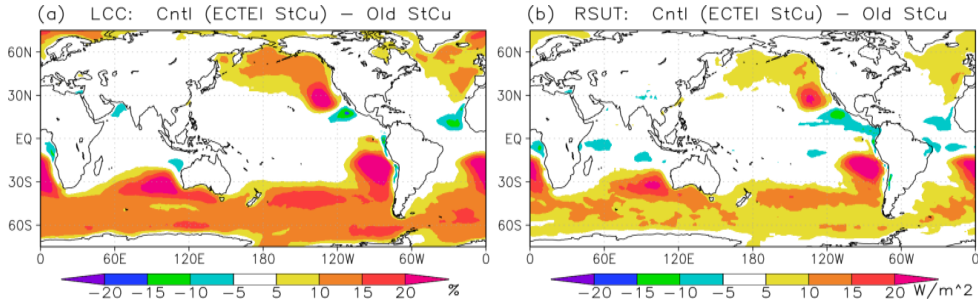
947 **Figure 2: Taylor diagrams for upward (a) shortwave, (b) longwave, and (c) net radiative fluxes at the top of the atmosphere for**
948 **MRI-CGCM3 (blue dot), MRI-ESM2 (red dot), the CMIP5 multi-model mean (black square), and individual CMIP5 models**
949 **(crosses). CERES-EBAF data are used as observations.**

950

951

952

953



954

955

956 **Figure 3: Impacts of the new stratocumulus scheme on (a) low cloud cover (%) and (b) TOA upward shortwave radiative flux (W**
957 **m^{-2}). The plots show results for the control model (with the new stratocumulus scheme) minus those for an experiment with an old**
958 **version of the stratocumulus scheme.**

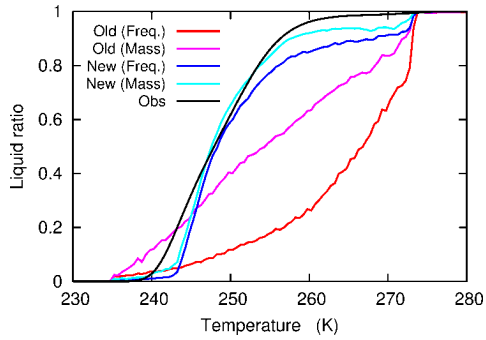
959

960

961

962

963



964

965

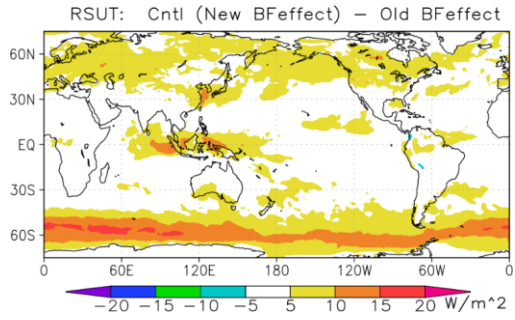
966 **Figure 4:** Ratio of super-cooled liquid water to total cloud water as a function of temperature. The plot is obtained from snapshot
967 global data for 10 days in July 2001 using the old (red and pink lines) and new (blue and light blue lines) treatments of the WBF
968 effect. The ratios are calculated using two methods: mass weighted ratio (pink and light blue lines) in which liquid and ice masses
969 are averaged over temperature bins first and the liquid water ratio is calculated from the averaged masses, and frequency ratio (red
970 and blue lines) in which the snapshot ratio of liquid water is weighted by snapshot cloud fraction and averaged over temperature
971 bins. An observational curve from Hu et al. (2010) that corresponds to a frequency ratio is also shown (black line).

972

973

974

975



976

977

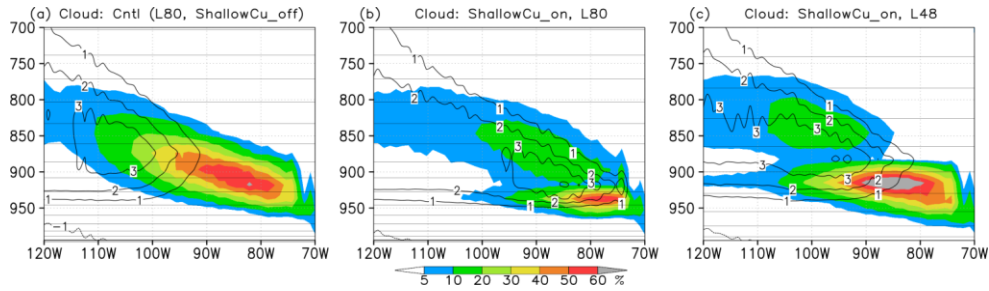
978 **Figure 5: Impact of the new treatment of the WBF effect on TOA upward shortwave radiative flux (W m^{-2}). The plot shows the**
979 **results for the control model (with the new treatment) minus those for an experiment with an old version of the treatment.**

980

981

982

983



984

985

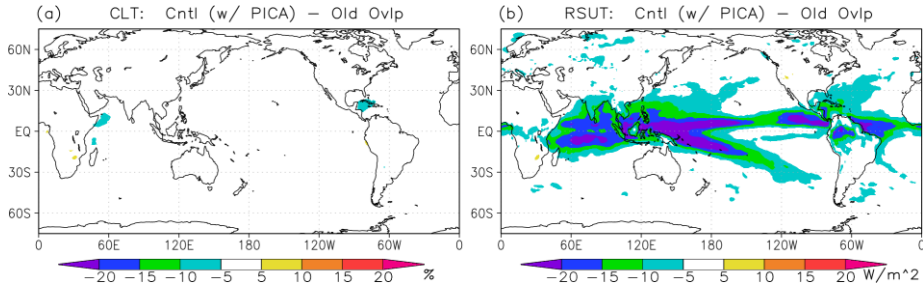
986 **Figure 6: Cross sections of cloud fraction (colour, %) along 20°S for January. (left) The control model (L80, a treatment of shallow**
987 **convection suppressed under stratocumulus conditions), (middle) the same as the left panel but where shallow convection can be**
988 **active even under stratocumulus conditions, and (right) the same as the middle panel except for vertical resolution L48. Horizontal**
989 **straight lines show the vertical model layers and contours show the heating rate of the convection scheme (K day^{-1}).**

990

991

992

993



994

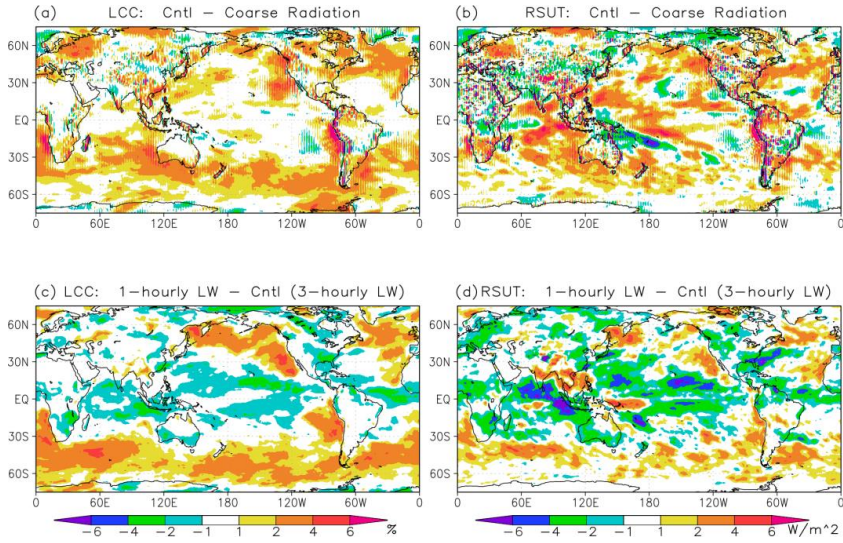
995

996 **Figure 7: Impacts of new cloud overlap scheme, PICA, for shortwave radiation calculation on (a) total cloud cover (%) and (b) TOA**
997 **upward shortwave radiative flux ($W m^{-2}$). The plots show results for the control model (with PICA) minus those for an experiment**
998 **with an old version of the cloud overlap scheme.**

999

1000

1001



1002

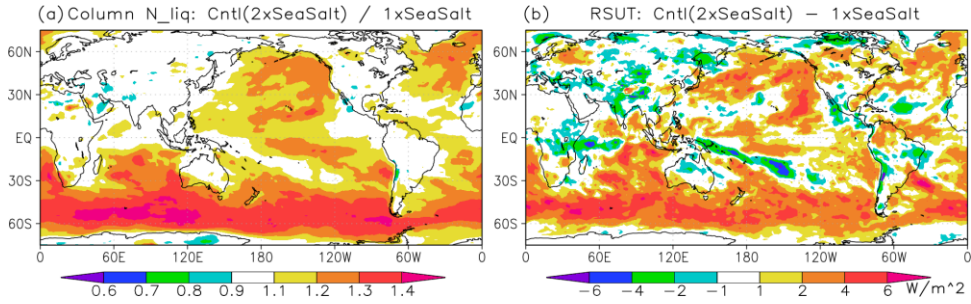
1003

1004 **Figure 8: Impacts of (a, b) increased horizontal resolution for the radiation calculation and (c, d) increased frequency of calculation**
1005 **for longwave radiation on (a, c) low cloud cover (%) and (b, d) TOA upward shortwave radiative flux ($W m^{-2}$).** Panels (a, b) show
1006 **results for the control model (calculation for every single grid box) minus those for an experiment with calculation for every two**
1007 **latitudinal grid boxes. Panels (c, d) show results for an experiment with 1-hourly longwave radiation calculation minus those for the**
1008 **control model (3-hourly calculation).**

1009

1010

1011



1012

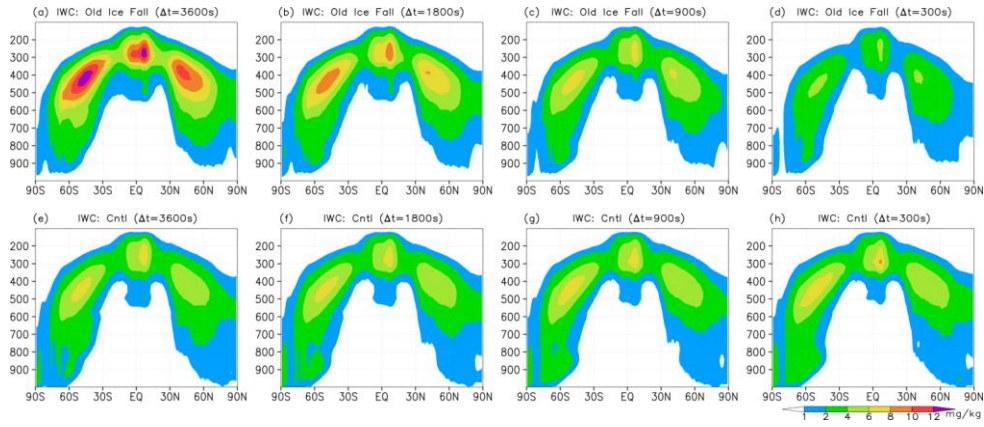
1013

1014 **Figure 9: Impacts of doubled number concentration of sea salt CCN on (a) column-integrated number concentration of cloud**
1015 **droplets (unitless) and (b) TOA upward shortwave radiative flux (W m^{-2}). The panels show the ratio (a) and the difference (b)**
1016 **between results for the control model (doubled number concentration of sea salt CCN) and those for an experiment using the original**
1017 **number concentration of sea salt CCN.**

1018

1019

1020



1021

1022

1023

1024

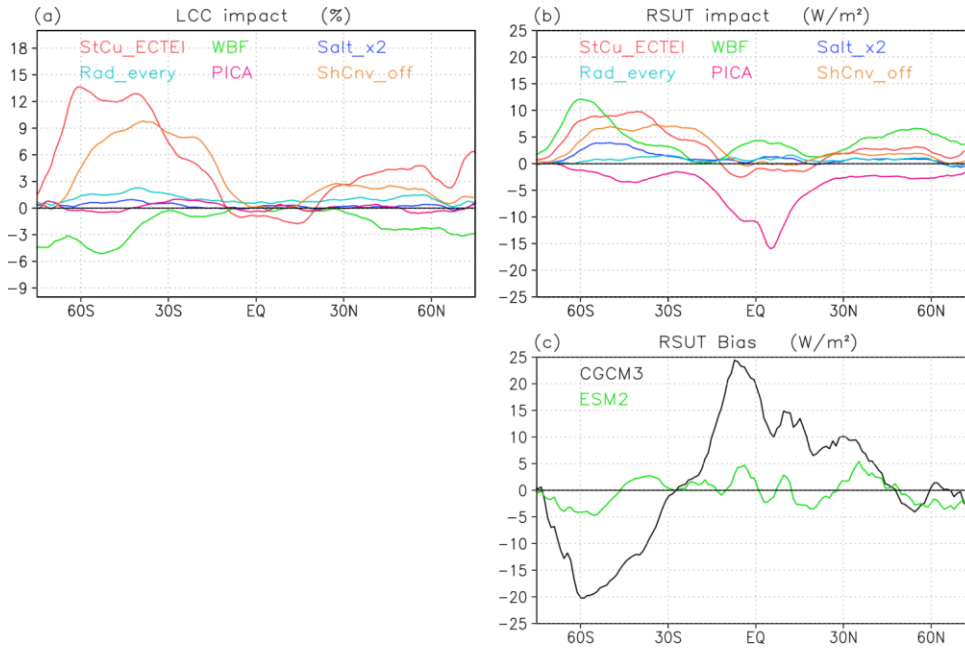
1025

1026

1027

Figure 10: Zonal average of ice water content (mg kg^{-1}) for different model time steps. Upper panels show results using the old ice fall scheme and lower panels the control simulation using the modified ice fall scheme. From left to right, the time steps are 3600 s, 1800 s, 900 s and 300 s. The vertical axis shows air pressure (hPa) and the horizontal axis shows latitude.

1028



1029

1030

1031

1032

1033

1034

1035

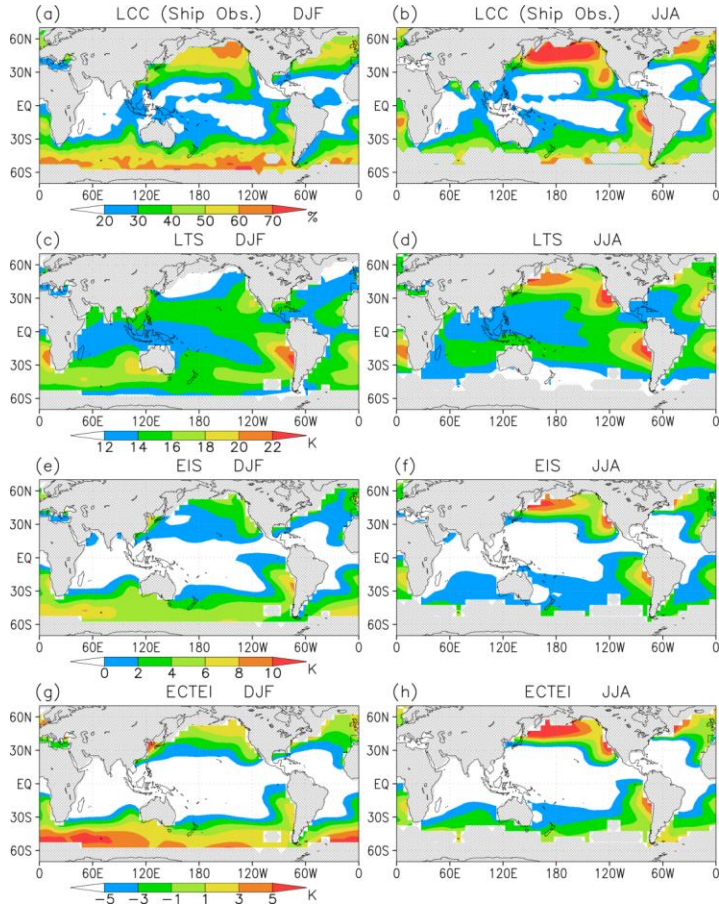
1036

1037

1038

Figure 11: Impacts of each modification on zonal means of (a) low cloud cover (%) and (b) TOA upward shortwave radiative flux (W m^{-2}). Modifications include a new stratocumulus scheme (red line), the new treatment of the WBF effect (green), doubled number concentration of sea salt CCN (blue), increased horizontal resolution for radiation calculation (light blue), a new cloud overlap scheme, PICA (pink), and a treatment of shallow convection suppressed under stratocumulus conditions (orange). Each impact is calculated from the simulation data described in Section 2.3. The biases in TOA upward shortwave radiative flux for MRI-CGCM3 (black line) and MRI-ESM2 (green) are also shown in panel (c), where the data used are the same as in Fig. 1.

1039



1040

1041

1042

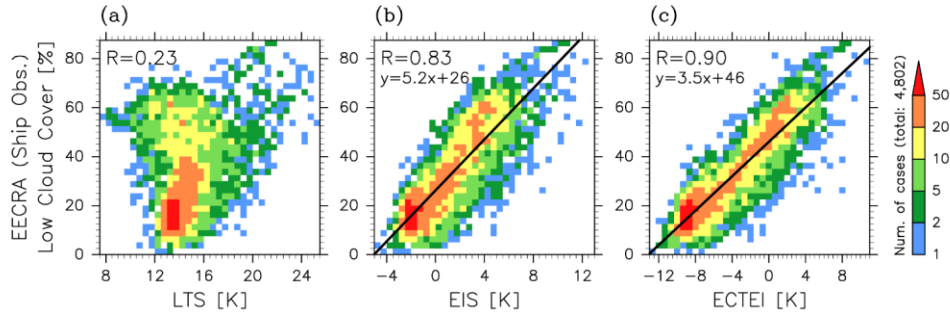
1043

1044

1045

Figure 12: Climatologies of low stratiform cloud cover (%), LTS (K), EIS (K), and ECTEI (K) for December to February (left panels) and June to August (right panels). Cloud cover data were obtained from EECRA shipboard observations and stability indexes were calculated using ERA-40 data (1957–2002).

1046



1047

1048

1049

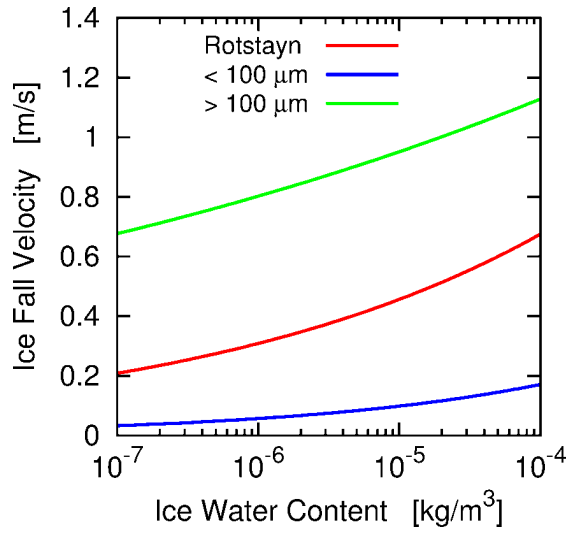
Figure 13: Frequencies of occurrence of low stratiform cloud cover (combined cloud cover of stratocumulus, stratus, and sky-obscuring fog) sorted by (a) LTS, (b) EIS, and (c) ECTEI ($\beta = 0.23$), based on all $5^\circ \times 5^\circ$ seasonal climatology data. Data are the same as in Fig. 12 but all the data between 60°N and 60°S for all seasons were used. Linear regression lines and the correlation coefficients are shown.

1052

1053

1054

1055



1056

1057

1058

1059

1060

1061

1062

Figure 14: Ice sedimentation velocities ($m s^{-1}$) of Rotstajn (1997) (Eq. (1), red line), derived for particles smaller than $100 \mu m$ (Eq. (3), blue line), and for particles larger than $100 \mu m$ (Eq. (4), green line). The horizontal axis shows ice water mass density $\rho_a q_i$ ($kg m^{-3}$).